Proteomic and Metabolomic Analyses of Atherosclerotic Vessels From Apolipoprotein E–Deficient Mice Reveal Alterations in Inflammation, Oxidative Stress, and Energy Metabolism

Manuel Mayr, Yuen-Li Chung, Ursula Mayr, Xiaoke Yin, Lucy Ly, Helen Troy, Salim Fredericks, Yanhua Hu, John R. Griffiths, Qingbo Xu

Objective—Proteomics and metabolomics are emerging technologies to study molecular mechanisms of diseases. We applied these techniques to identify protein and metabolite changes in vessels of apolipoprotein $E^{-/-}$ mice on normal chow diet.

Methods and Results—Using 2-dimensional gel electrophoresis and mass spectrometry, we identified 79 protein species that were altered during various stages of atherogenesis. Immunoglobulin deposition, redox imbalance, and impaired energy metabolism preceded lesion formation in apolipoprotein $E^{-/-}$ mice. Oxidative stress in the vasculature was reflected by the oxidation status of 1-Cys peroxiredoxin and correlated to the extent of lesion formation in 12-month-old apolipoprotein $E^{-/-}$ mice. Nuclear magnetic resonance spectroscopy revealed a decline in alanine and a depletion of the adenosine nucleotide pool in vessels of 10-week-old apolipoprotein $E^{-/-}$ mice. Attenuation of lesion formation was associated with alterations of NADPH generating malic enzyme, which provides reducing equivalents for lipid synthesis and glutathione recycling and successful replenishment of the vascular energy pool.

Conclusion—Our study provides the most comprehensive dataset of protein and metabolite changes during atherogenesis published so far and highlights potential associations of immune-inflammatory responses, oxidative stress, and energy metabolism. (***Arterioscler Thromb Vasc Biol.*** **2005;25:0-0.**)

Key Words: animal model ■ apolipoprotein E ■ atherosclerosis ■ metabolomics ■ oxidative stress ■ proteomics

The generation of apolipoprotein E–deficient (apolipoprotein $E^{-/-}$) mice[1,2] has been one of the most critical advancements in the elucidation of factors affecting atherogenesis. It is currently the most popular murine model in cardiovascular research and has revealed important insights into atherosclerosis. But despite a decade of research, there is still a need for sophisticated experimental techniques to obtain a more comprehensive understanding of the complex pathophysiology.[3] Previous studies have revealed apolipoprotein E-related alterations in the transcriptome.[4] However, simple deduction of protein expression from mRNA transcript analysis is insufficient[5] and, importantly, provides no information on post-translational modifications, which are known to be instrumental in many human diseases.

We recently analyzed the proteomic profile of mouse arterial smooth muscle that was markedly influenced by mutational ablation of the PKCΔ gene.[6] Our proteomic findings were translated into a functional context by combining proteomics with metabolomic techniques, under in vivo[7,8] as well as in vitro conditions.[6] This new research strategy allows us to decipher dynamic alterations of cellular proteins and metabolites revealing multiple facets of a single pathogenesis.[9]

In vascular research, proteomics and metabolomics are still in their infancies. Human umbilical cord endothelial cells and arterial and saphenous vein medial smooth muscle have been scantily characterized, but most attempts to apply proteomic techniques to human atheroma were jeopardized by the accumulation of serum proteins and the genetic heterogeneity of human samples, as summarized in a recent review article.[9] Thus, we decided to use a mouse model, which offers the opportunity to analyze protein changes during various stages of atherogenesis under well-defined laboratory conditions and in animals with identical genetic background facilitating proteomic comparisons by limiting biological variation.

Materials and Methods

Mice

All procedures were performed according to protocols approved by the Institutional Committee for Use and Care of Laboratory Animals.

Original received March 29, 2005; final version accepted August 15, 2005.

From the Departments of Cardiac and Vascular Sciences (M.M., U.M., X.Y., L.L., S.F., Y.H., Q.X.) and Basic Medical Sciences (Y.-L.C., H.T., J.R.G.), St George's, University of London, UK.

Correspondence to Dr Manuel Mayr, Department of Cardiac and Vascular Sciences, St George', University of London, UK, Cranmer Terrace, London SW17 0RE, UK. E-mail m.mayr@sgul.ac.uk

Arterioscler Thromb Vasc Biol. **is available at http://www.atvbaha.org** **DOI: 10.1161/01.ATV.0000183928.25844.f6**

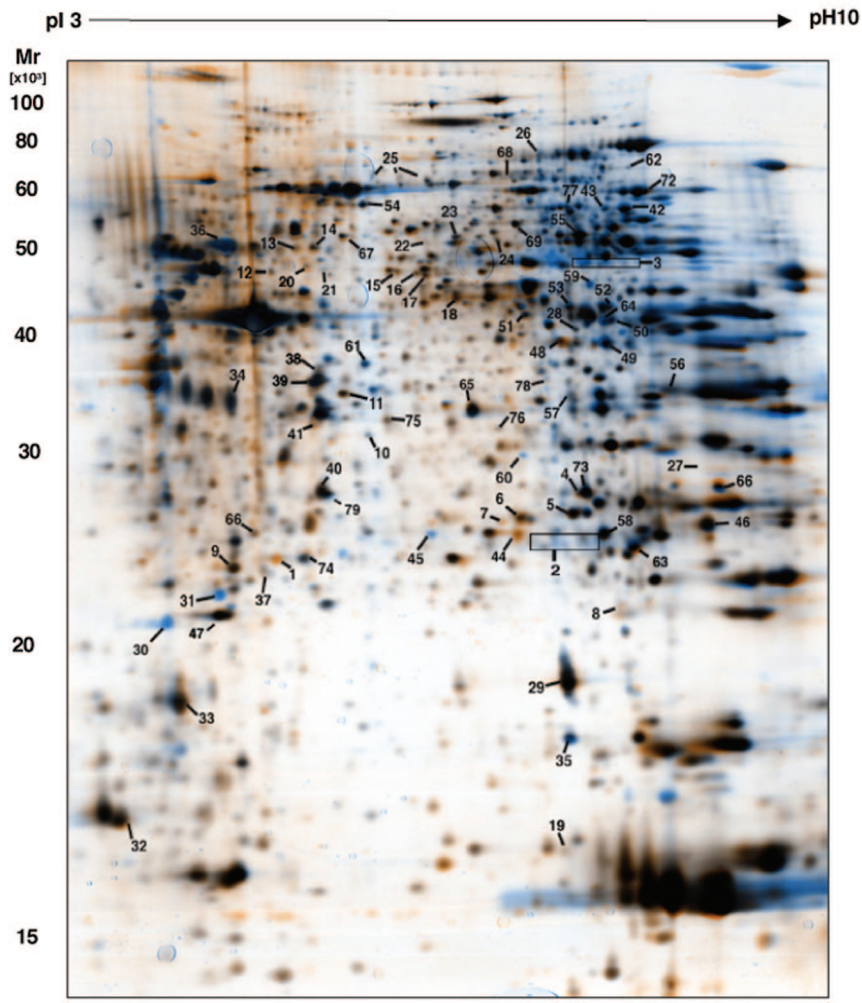

Figure 1. 2D map of proteins expressed in aortas of 10-week-old apolipoprotein $E^{+/+}$ and apolipoprotein $E^{-/-}$ mice. Protein extracts were separated on a pH 3 to 10NL IPG strip, followed by a 12% SDS polyacrylamide gel. Spots were detected by silver staining. The figure represents a direct overlay of average gels from apolipoprotein $E^{+/+}$ and apolipoprotein $E^{-/-}$ vessels. Average gels were created from 4 single gels (total n=8). Differentially expressed spots are highlighted in color (orange and blue for apolipoprotein $E^{+/+}$ and apolipoprotein $E^{-/-}$ vessels, respectively). Proteins identified by mass spectrometry are marked with numbers and listed in Table I.

Apolipoprotein E–deficient mice on a C57BL/6 background were purchased from Jackson Laboratories (West Grove, Pa) and maintained in our laboratory. Mice were fed a normal chow diet containing 4.5% fat by weight (0.02% cholesterol) and kept on a light/dark (12/12-hour) cycle at 22°C, receiving food and water ad libitum.

Assessment of Lesion Formation

Aortas from 10-week-old, 12-month-old, and 18-month-old mice were dissected from the brachiocephalic trunk to the iliac bifurcation. Macroscopically, no lesions were observed on the aortic surface of 10-week-old apolipoprotein $E^{-/-}$ mice. Aortic lesions in 12-month-old mice were quantified by estimating the lesion-covered area on the aortic surface (as percent of surface area) and were classified as light (<10%), medium (10% to 30%), and severe (>30%). Disease severity was further verified by oil red O staining of the aortic root (measured as averaged lesion per cross-section of the aortic sinus). The frequency of light, moderate and severe lesions in 12-month-old apolipoprotein $E^{-/-}$ mice on normal chow diet was ≈40%, 50%, and 10%, respectively. At 18 months, most apolipoprotein $E^{-/-}$ mice had severe lesions in their arteries.

Proteomic and Metabolomic Analysis

For proteomic and metabolomic analyses, aortas were rinsed thoroughly with cold phosphate-buffered saline to remove any blood components and frozen immediately in liquid nitrogen (LN_2). Aortas from both sexes were used in all experiments. A detailed methodology is available online (http://atvb.ahajournals.org). Protocols can be downloaded from our website (www.vascular-proteomics.com).

Standard Methods

Western blotting, immunohistochemistry, and enzymatic assays are available online at http://atvb.ahajournals.org.

Statistical Analysis

Statistical analysis was performed using the analysis of variance and Student *t* test. Pairwise comparisons between metabolites were performed using the Bonferroni/Dunn test. Results were given as means±SE. $P<0.05$ was considered significant.

Results

Proteomic Analysis

To analyze changes in the proteome, we created protein profiles of aortas by 2-DE. Aortas were derived from 10-week-old and 12-month-old apolipoprotein $E^{+/+}$ and apolipoprotein $E^{-/-}$ mice. Average gels were obtained from at least 4 animals per group. A direct overlay is presented in Figure 1. Using a broad range pH gradient (pH 3 to 10 NL), 2-DE gels compromised ≈1500 protein features. Differentially expressed spots are highlighted in color (orange and blue indicate an increase in aortas of apolipoprotein $E^{+/+}$ and apolipoprotein $E^{-/-}$ mice, respectively). Numbered spots were excised and subject to in-gel tryptic digestion. Protein identifications as obtained by mass spectrometry are listed in Table I (available online at http://atvb.ahajournals.org). For

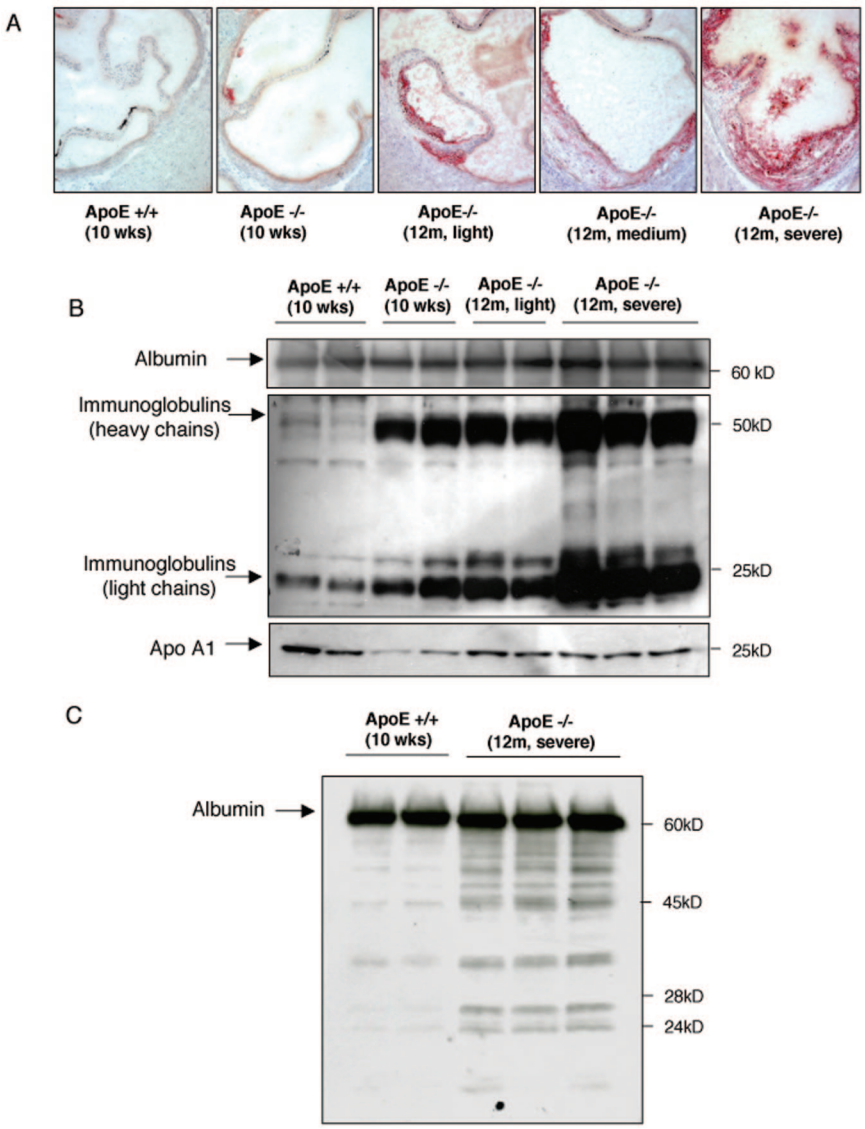

Figure 2. Atherosclerotic lesions in apolipoprotein $E^{-/-}$ mice. A, Representative photographs of oil red O-stained sections from aortic roots, indicating lesions (red color) of 10-week-old apolipoprotein $E^{+/+}$ and apolipoprotein $E^{-/-}$ mice and 12-month-old apolipoprotein $E^{-/-}$ mice with light, medium, and severe disease. Original magnification ×100. B and C, Western blots probed with antibodies to albumin, immunoglobulins, and apolipoprotein A1. Note that albumin undergoes extensive fragmentation in advanced lesions (C) and that immunoglobulins were barely detectable in apolipoprotein $E^{+/+}$ aortas, but abundant in apolipoprotein $E^{-/-}$ vessels (B).

spots marked with an asterisk (*), further proof of identification was obtained by tandem mass spectrometry (n=38; Table II, available online at http://atvb.ahajournals.org). Representative spectra are shown online.

To quantitatively monitor protein changes during atherogenesis, aortas of 12-month-old apolipoprotein $E^{-/-}$ mice were classified according to their atherosclerotic surface area in vessels with light (<10%), medium (10% to 30%), and severe atherosclerosis (>30%). Confirmation was provided by oil red O staining (Figure 2A). Cholesterol levels were significantly increased in all subgroups of chow-fed apolipoprotein $E^{-/-}$ mice compared with wild-type controls ($P<0.001$ ANOVA), but no correlation was observed between cholesterol levels and disease severity in 12-month-old apolipoprotein $E^{-/-}$ mice (449±49 and 421±127 mg/dL in animals with light and severe lesions, respectively), which is in line with previous reports.[10] Quantitative data on protein changes during disease progression are summarized in Table III (available online at http://atvb.ahajournals.org).

Accumulation of Serum Components

As expected, macrophage markers (MAC2, CapG) increased, whereas SMC markers (SM22) decreased, and serum proteins accumulated with lesion progression, including fibrinogen, transferrin, and hemopexin. Interestingly, immunoglobulin deposits were barely detectable in apolipoprotein $E^{+/+}$ mice, but abundant even in aortas of young apolipoprotein $E^{-/-}$ mice (Figure 2B), forming 2 charge trains of molecular masses 25 700 and 50 800 Da with pI values of 7.8 to 5.8 on 2D gels. Whereas further immunoglobulin deposition occurred during lesion progression, albumin was subject to extensive fragmentation within advanced atherosclerotic plaques (Figure 2C). Apolipoprotein A1 (apoA1), the major protein fraction of high-density lipoprotein, whose protective anti-oxidative role in the cardiovascular system is well-established, was significantly reduced in aortas of apolipoprotein $E^{-/-}$ mice (Figure 2B).

Increased Oxidative Stress

Besides revealing differences in protein expression, 2D gel electrophoresis has the potential to display differences in

posttranslational modifications. Redox-active cysteines constitute the main antioxidative component of peroxiredoxins.[11] This protein family represents a special type of peroxidase as the protein is the reducing substrate itself; on oxidative stress, the cysteine in the active site is either oxidized to cysteine sulfenic acid or overoxidized to cysteine sulfinic acid. Whereas the first modification is DTT-sensitive and therefore undetectable in 2-DE gels, the latter modification is DTT-resistant and results in a charge shift toward a more acidic pI.[12] Thus, peroxiredoxins are often encountered as doublet spots in 2-DE and the ratio of oxidized to reduced protein is a reliable surrogate marker for oxidative stress.[11,12]

1-Cys peroxiredoxin (1-Cys prx), a novel antioxidant conferring protection against oxidative membrane damage,[13] was almost exclusively present as a reduced (basic) isoform in apolipoprotein $E^{+/+}$ aortas, whereas oxidation of 1-Cys prx was detectable in vessels of young apolipoprotein $E^{-/-}$ mice, resulting in decreased abundance of the reduced isoform (Figure 3A). Consequently, the ratio of oxidized to reduced 1-Cys prx was 15-times higher in young apolipoprotein $E^{-/-}$ mice compared with wild-type controls (0.58 ± 0.18 versus 0.04 ± 0.03; $P<0.05$). Surprisingly, it temporarily normalized in vessels harboring light lesions (0.10 ± 0.06 versus 0.04 ± 0.03, nonsignificant); however, overall, there appeared to be a linear relationship between the extent of oxidation of 1-Cys prx and the extent of lesion formation in aortas of 12-month-old apolipoprotein $E^{-/-}$ mice (Figure 3A).

Antioxidant Defense

1-Cys prx is able to reduce peroxidised membrane phospholipids by using glutathione (GSH) as a reductant.[13] Under oxidative stress, GSH is oxidized to GSSG and subsequently reduced by GSH reductase through the coupling reaction of NADPH to NADP. Strikingly, GSH reductase activity was found to be increased in aortas of young apolipoprotein $E^{-/-}$ mice (78.4 ± 12.4 IU/L versus 37.9 ± 1.4 IU/L; n=3; $P<0.05$) and the oxidation state of 1-Cys prx in 12-month-old apolipoprotein $E^{-/-}$ mice correlated to the expression pattern of the cytosolic isoform of malic enzyme (MOD-1), which generates cytosolic NADPH,[14] providing reducing equivalents for lipid synthesis and GSH recycling (Figure 3B). Aortas harboring only light lesions demonstrated a prominent change in MOD-1 (Figure 3B) associated with decreased oxidation of 1-Cys prx (Figure 3A), lower levels of the oxidative stress-induced protein HO-1 (Figure 4A and 4B), and a trend to higher GSH concentrations compared with age-matched vessels with advanced disease (42 ± 0.9 versus 31 ± 0.8 nmol/g wet weight; n=3; $P=0.10$). In contrast, upregulation of antioxidant proteins was only detectable in advanced, but not early, stages of disease (Figure 4A). This is consistent with previously published mRNA data, reporting decreased antioxidant transcription in aortas of apolipoprotein $E^{-/-}$ mice at the onset of lesion formation.[15]

Enzymatic Changes

Among the differentially expressed proteins were several glycolytic enzymes, including triose phosphate isomerase, transketolase, glyceraldeyde-3-phosphate dehydrogenase, enolase, and phosphoglycerate mutase, as well as all 3 subunits of the pyruvate dehydrogenase complex, which accomplishes the irreversible step from glycolysis to the trichloroacetic acid (TCA) cycle by converting pyruvate to acetyl-coenzyme A (CoA). Changes of enzymes involved in glucose metabolism were accompanied by a reduction of cytoplasmic malate dehydrogenase, which is involved in the transfer of cytosolic NADH into mitochondria. Concomitantly, short chain–specific acyl-CoA dehydrogenases, responsible for the degradation of short chain fatty acids to acetyl-CoA, were differentially expressed in aortas of young apolipoprotein $E^{-/-}$ mice and medium chain–specific acyl-CoA dehydrogenases became upregulated in vessels of old apolipoprotein $E^{-/-}$mice (Table III).

Metabolite Changes

To clarify the metabolic net effect of these enzymatic changes, we measured vascular metabolites by high-resolution NMR spectroscopy. A representative ^{1}H MR spectrum of an aortic extract is shown in Figure 5. Quantitative data are included as Table IV (available online at http://atvb.ahajournals.org), whereas Figure 6 shows a histogram displaying the relative metabolite ratios for apolipoprotein $E^{-/-}$ aortas derived from 10-week-old and 18-month-old apolipoprotein $E^{-/-}$ mice compared with wild-type controls. Decreased concentrations of alanine, a transamination product of pyruvate, were associated with a reduction of the adenosine nucleotide pool in aortas of young apolipoprotein $E^{-/-}$ mice and a coordinated but nonsignificant decline of other energy metabolites, such as total creatine and succinate, the oxidation of which is directly associated with respiratory chain reactions. The ratio of alanine to pyruvate was significantly decreased in young apolipoprotein $E^{-/-}$ mice compared with wild-type controls (1.7 ± 0.8 versus 7.5 ± 1.6; $P=0.002$) and remained reduced in old apolipoprotein $E^{-/-}$ mice (4.1 ± 1.7 versus 7.5 ± 1.6, $P=0.019$, respectively), but the adenosine nucleotide and creatine pool normalized. The metabolic profiles also revealed a significant increase in choline in aortas of old apolipoprotein $E^{-/-}$ mice. Interestingly, concentrations of trimethylamino oxide, a breakdown product of choline, were significantly higher in male than female aortas, suggesting a gender-specific difference in choline metabolism, which was independent of the apolipoprotein E genotype (inset in Figure 6). An additional comparison of metabolic profiles obtained from sex-matched aortas of 12-month-old apolipoprotein $E^{-/-}$ mice (n=3 in each group, 2 males, 1 female) revealed that aortas harboring only light lesions had a 1.7- and 1.9-fold increase in adenosine nucleotides ($P=0.028$) and succinate ($P=0.060$), respectively, but only half the glucose concentration ($P=0.109$) compared with aortas with severe disease.

Discussion

Our study provides evidence that immune activation, oxidative stress, and energetic impairment are among the earliest alterations in hyperlipidemic animals.

Inflammation

Immunoglobulin deposition within the vessel wall of apolipoprotein $E^{-/-}$ mice is close to peak levels even before lesion

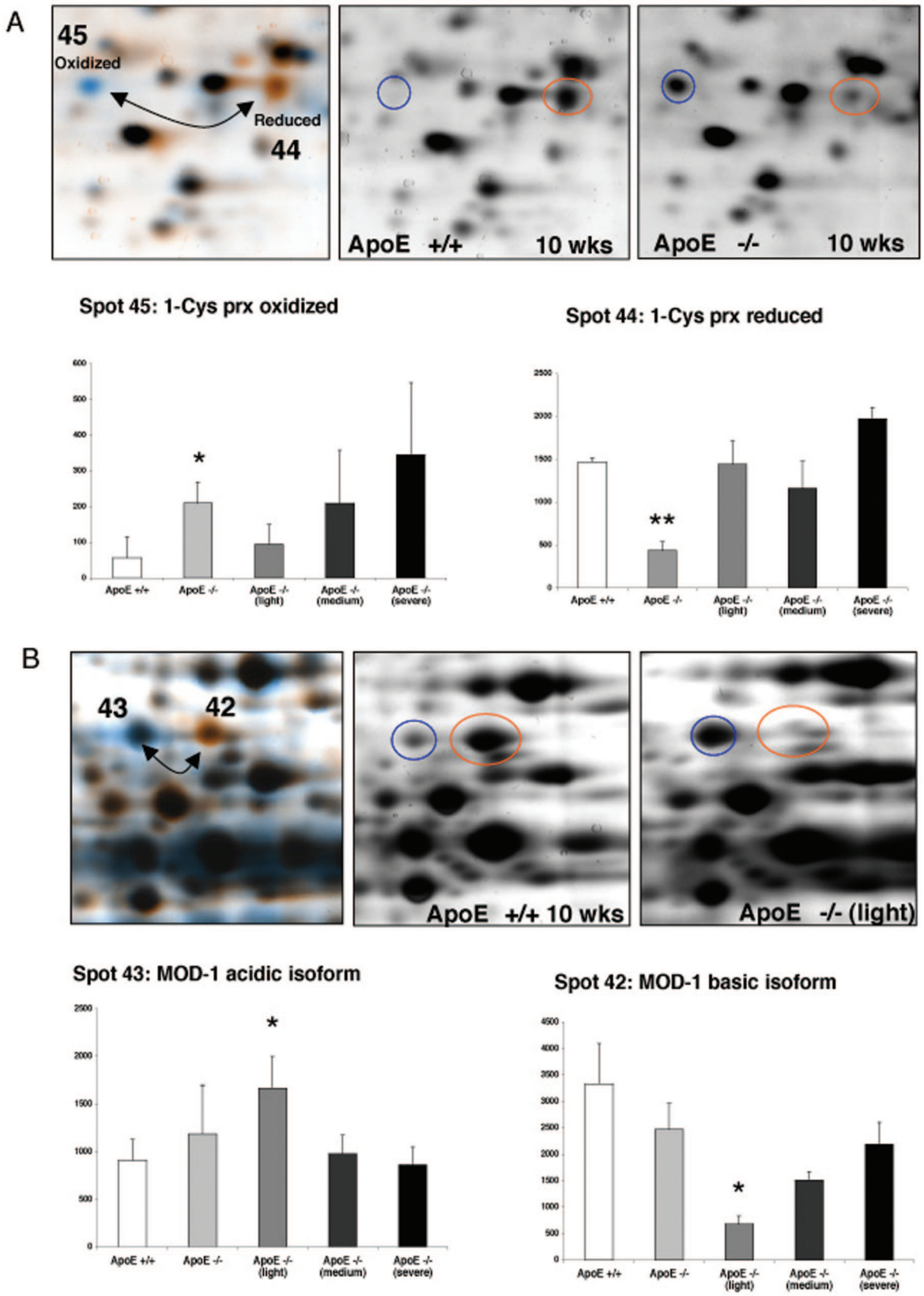

Figure 3. Oxidative stress in apolipoprotein $E^{-/-}$ aortas. The spot pair corresponding to 1-Cys peroxiredoxin (1-Cys-Prx) is marked with an arrow (A). Numbers correspond to protein identities in Table I. Quantitative changes in expression of the oxidized and reduced form of 1-Cys prx during atherogenesis are shown below. Note that 1-Cys-Prx is predominantly present as reduced protein in apolipoprotein $E^{+/+}$ vessels but is oxidized in apolipoprotein $E^{-/-}$ vessels. Expression pattern of malic enzyme supernatant (MOD-1) (B). *Significant difference to wild-type controls, $P<0.05$, ** $P<0.01$.

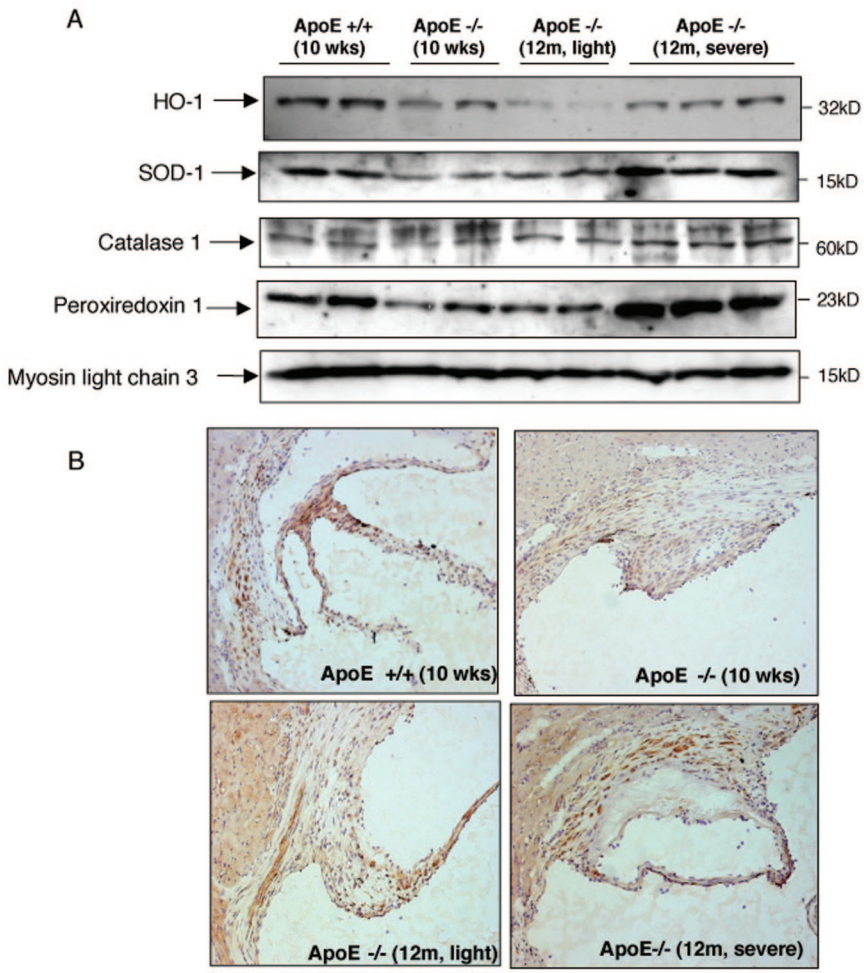

Figure 4. Antioxidants in apolipoprotein $E^{-/-}$ aortas. Western blot analysis to determine expression levels of antioxidant proteins in aortic tissues, including heme oxygenase-1 (HO-1), superoxide dismutase-1 (SOD-1), catalase 1, and peroxiredoxin 1 (A). Note that HO-1 expression is higher in aortas with advanced atherosclerosis compared with age-matched vessels harboring only light lesions (B).

formation initiates and cannot be accounted for by impaired endothelial barrier function, because other serum components, such as albumin and fibrinogen, did not accumulate in vessels without overt atherosclerosis. In murine models, antibodies recognizing oxidized phospholipids correlate closely with lesion progression and regression[16–18] and a class shift from IgG2a to IgG1, indicative for a switch of the T-cell response from Th1 to Th2, has been observed for circulating oxidized low-density lipoprotein antibodies in apolipoprotein $E^{-/-}$ mice.[19] Similarly, we observed a preponderance of IgG1 within atherosclerotic lesions and mass spectrometry data obtained from the variable region of accumulated immunoglobulins suggest that at least some are directed against phosphocholine (gi30720232, anti-phosphocholine immunoglobulin heavy chain variable region [mus musculus], sequence coverage 33%). However, further studies will be required to allow for a more detailed characterization.

Oxidative Stress

Oxidative stress, the local imbalance between the ubiquitous formation of reactive oxygen species (ROS) and the equally ubiquitous antioxidant defenses, is thought to play an important role in vascular injury and atherogenesis.[20–22] The complexity of the antioxidant defense have made it difficult to assess their impact on atherosclerosis as it is likely that knockout of individual ROS-generating or ROS-scavenging enzymes are compensated for by synergistic ones.[23] Because the pathogenetic outcome is determined by the balance between pro-oxidants and antioxidants, measurements of individual enzymes at a single time are unlikely to shed much light and a more comprehensive approach is needed.[23]

Our proteomic data support the role of oxidative stress in atherogenesis: First, oxidation of 1-Cys prx, a reliable in vivo marker of oxidative stress,[11,12] was significantly elevated in young apolipoprotein $E^{-/-}$ mice compared with wild-type controls. Second, the oxidation state of 1-Cys prx correlated to lesion size in aortas of 12-month-old mice indicating that reduced oxidative stress might attenuate lesion progression in apolipoprotein $E^{-/-}$ mice. Third, the observed reduction of oxidative stress in vessels with light lesions was not a result of increased expression of antioxidants, because protein levels of catalase 1, SOD-1, and peroxiredoxin 1 were similar to those in young apolipoprotein $E^{-/-}$ mice. The oxidation status of 1-Cys prx, however, showed a striking correlation to proteomic changes of malic enzyme supernatant (MOD-1). As demonstrated previously, such changes in the protein pattern are likely to reflect alterations in enzymatic activity.[6–9] The soluble form of malic enzyme is 1 of 3 enzymes, apart from glucose 6-phosphate dehydrogenase and cytoplasmic isocitrate dehydrogenase, that can generate cytosolic NADPH,[14] providing reducing equivalents for lipid synthesis,

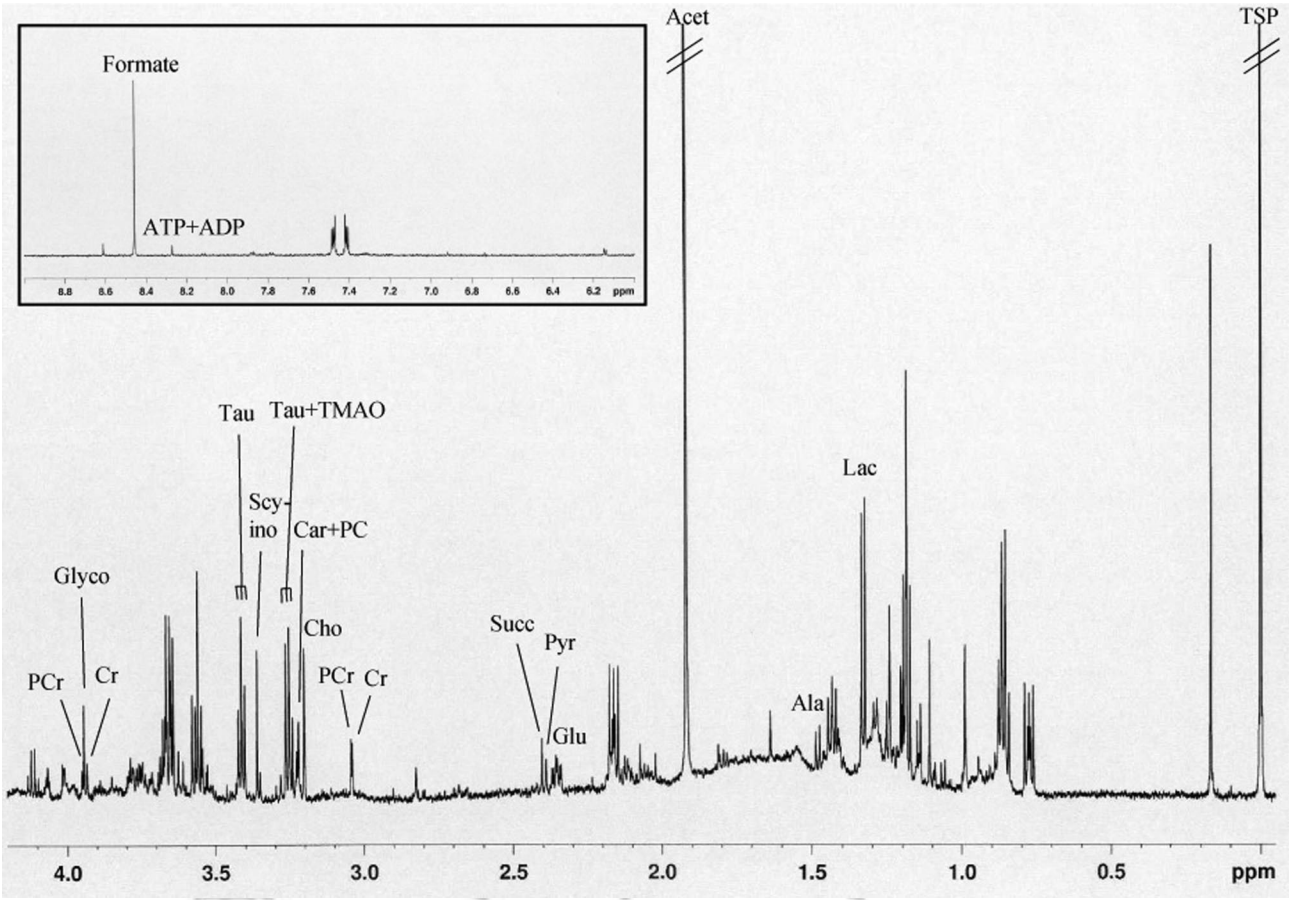

Figure 5. NMR spectra of a murine aorta derived from 18-month-old apolipoprotein $E^{-/-}$ mice. Within the aliphatic region (−0.05 to 4.2 ppm) of the NMR spectra, resonances have been assigned to lactate (Lac), alanine (Ala), pyruvate (Pyr), acetate (Acet), succinate (Succ), carnitine (Car), choline (Cho), phosphocholine (PC), taurine (Tau), scyllo-inositol (Scy-ino), glycolic acid (Glyco), trimethylamino oxide (TMAO), glutamate (Glu), creatine (Cr), phosphocreatine (PCr). ADP+ATP and formate are showing in the aromatic region of the spectra (6.0 to 9.0 ppm, see insert).

as well as for glutathione and thioredoxin reductase, which are of paramount importance in maintaining the reducing intracellular environment.[24,25] The importance of thiol-based defense mechanisms in hyperlipidemia is supported by the increase in glutathione reductase activity in vessels of young apolipoprotein $E^{-/-}$ mice. This initial glutathione defense appears to be overwhelmed in advanced stages of disease as indicated by a rebound in the oxidation of 1-Cys prx, increased expression of HO-1, and lower glutathione levels compared with aortas harboring light lesions. Thus, upregulation of antioxidant proteins appears to be the last resort, once other counter-regulatory mechanisms cannot provide sufficient reducing equivalents to antagonize ROS, rather than the first attempt to confine oxidative stress. These findings would be consistent with previous studies reporting a weak glutathione-related enzymatic antioxidant shield in human atheroma.[26]

Despite a conjunct upregulation of antioxidant proteins in advanced stages of disease, deleterious consequences of reactive oxygen species became apparent, such as proteolysis of oxidatively damaged proteins.[27] Albumin is degraded 50-times faster on oxidation,[27,28] providing a possible explanation for its extensive fragmentation. Similarly, enzymes known to be susceptible to free radical-mediated inactivation such as aconitase and the Rieske protein of ubiquinol cytochrome C reductase, which contain iron–sulfur centers, a coordination complex with cysteine sulfurs of proteins, were altered in advanced stages of atherosclerosis.[29,30] Such interactions are of potential importance, as damage to such complexes results in release of free iron and subsequent formation of hydroxyl radical, a highly reactive oxygen species, which perpetuates the vicious cycle of oxidative stress.[31]

Energy Metabolism

Metabolic disturbances are likely to be a key factor in both the initiation and progression of atherosclerosis. The upregulation of acyl-CoA dehydrogenases, the decrease in alanine, a transamination product of pyruvate, and the downregulation of cytoplasmic malate dehydrogenase, responsible for transferring cytosolic NADH produced during glycolysis into mitochondria,[32] suggest that vascular cells might respond to hyperlipidemia by metabolizing lipids instead of glucose. Increased fatty acid oxidation would exert a negative feedback on the activity of the pyruvate dehydrogenase complex[32] slowing down glucose metabolism, the main source of energy for the vasculature.[33] Moreover, when excess fatty acids reach mitochondria, there is even a risk of uncoupling

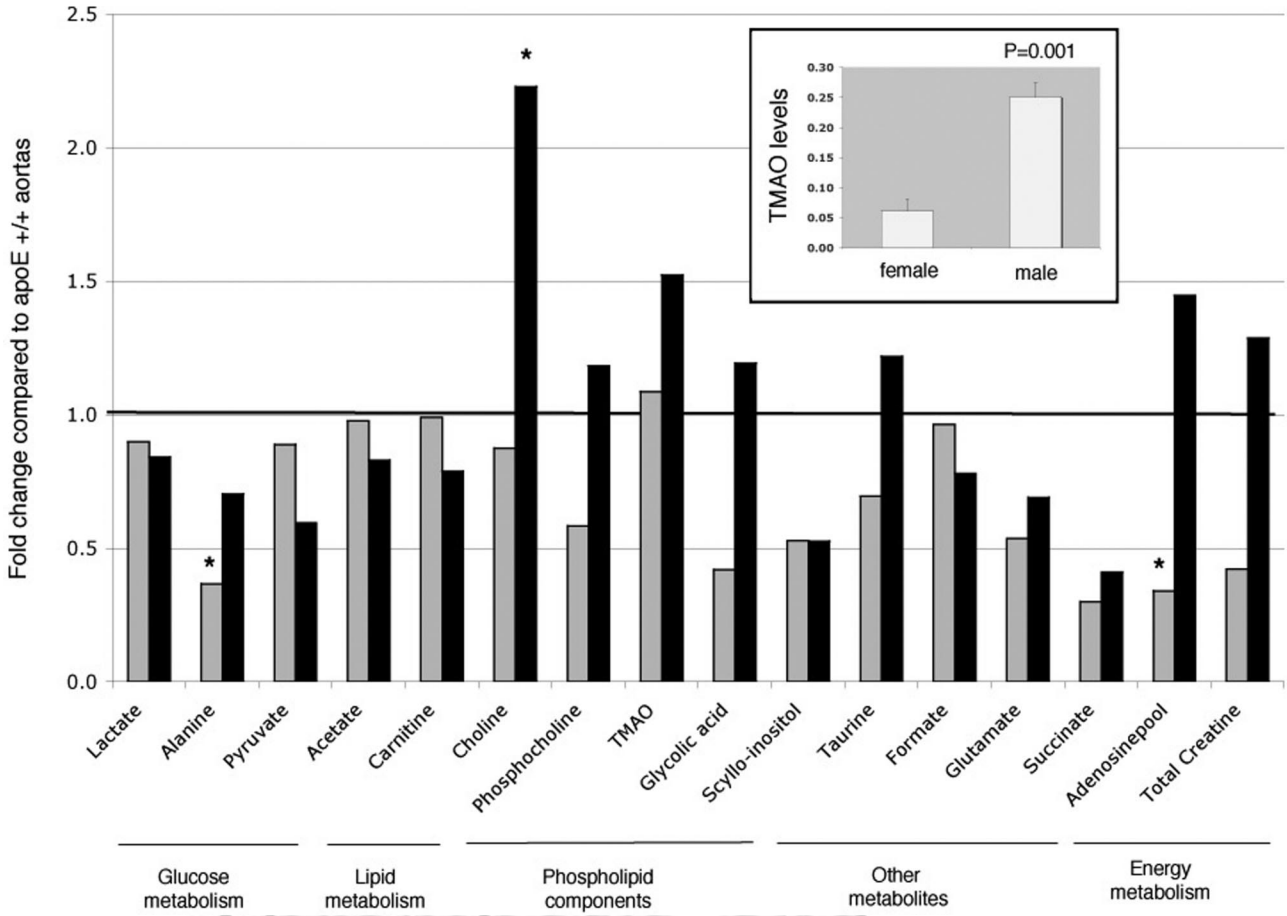

Figure 6. Comparison of metabolites in apolipoprotein $E^{+/+}$ and apolipoprotein $E^{-/-}$ aortas. Relative changes of metabolites in aortas derived from 10-week-old (gray bars) and 18-month-old (black bars) apolipoprotein $E^{-/-}$ aortas compared with apolipoprotein $E^{+/+}$ aortas (reference line). Abbreviations for metabolites are explained in the legend to Figure 5. Data are provided in Table IV. The inset highlights a gender difference for TMAO concentrations in murine aortas. *Significant difference with Bonferroni/Dunn, $P<0.017$.

oxidation from phosphorylation with oxygen wastage.[32] Insufficient phosphorylation of energy metabolites will cause their degradation and tissue depletion, providing a possible explanation for the observed reduction of the adenosine nucleotide pool in young apolipoprotein $E^{-/-}$ mice. Notably, breakdown products of adenosine, xanthine and hypoxanthine, both substrates for the xanthine oxidase, are a powerful enzyme in the generation of ROS.[34] It is noteworthy that the depletion of vascular energy metabolites coincided with increased oxidation of 1-Cys prx in young apolipoprotein $E^{-/-}$ mice, whereas attenuated lesion formation in 12-month-old apolipoprotein $E^{-/-}$ mice was associated with reduced oxidative stress and successful recovery of the adenosine nucleotide pool possibly serviced by increased glucose use. Supporting our findings are previous observations that insulin supplementation reduces lesion formation and oxidative stress in apolipoprotein $E^{-/-}$ mice[35]. In contrast, overexpression of the uncoupling protein 1 results in mitochondrial dysfunction and promotes atherosclerosis by depleting energy stores and increasing superoxide production.[36] Thus, there is evidence that inefficient glucose and energy metabolism may contribute to oxidative stress and vascular disease in hyperlipidemic mice.

Study Limitation

A main obstacle for applying proteomic analysis to vascular pathology is the heterogeneous cellular composition of atherosclerotic plaques. Whereas smooth muscle cells dominate proteomic profiles of normal vessels, advanced lesions contain large numbers of monocyte-derived macrophages. Overall, the proteomic profiles were remarkably consistent in young and old apolipoprotein $E^{-/-}$ mice: only 2 macrophage proteins, namely CapG, which accounts for 0.6% of total macrophage proteins, and MAC-2, which is also abundant in activated macrophages, showed a significant increase in advanced stages of disease, indicating that the concentration of other macrophage proteins in aortic extracts was not high enough to allow detection on 2D gels. Thus, the proteomic and metabolic profiles remain dominated by vascular smooth muscle cells, facilitating data interpretation.

Finally, we should point out that our proteomic analysis revealed differential expression of several signaling proteins, but the vascular function of some proteins, eg, dihydropyrimidinase-like proteins 2 and 3, which are regulators of neuronal development and axonal outgrowth,[37] is currently unknown. For others, there is evidence for their involvement in atherosclerosis: downregulation of Ras sup-

pressor protein 1, an endogenous inhibitor of the Ras signaling pathway, during lesion progression, is consistent with a study reporting attenuation of lesion formation in apolipoprotein $E^{-/-}$ by inhibiting the Ras signaling pathway;[38] the functional relevance of 14 to 3-3 gamma, an inhibitor of the protein kinase C signaling pathway, is supported by our findings that deficiency for protein kinase Cδ accelerates neointima formation in a mouse model of vein graft arteriosclerosis.[39]

Acknowledgments

The use of the facilities of the Medical Biomics Centre at St. George's, University of London, is gratefully acknowledged. This work was supported by grants from British Heart Foundation and the Oak Foundation.

References

1. Zhang SH, Reddick RL, Piedrahita JA, Maeda N. Spontaneous hypercholesterolemia and arterial lesions in mice lacking apolipoprotein E. *Science*. 1992;258:468–471.
2. Plump AS, Smith JD, Hayek T, Aalto-Setala K, Walsh A, Verstuyft JG, Rubin EM, Breslow JL. Severe hypercholesterolemia and atherosclerosis in apolipoprotein E-deficient mice created by homologous recombination in ES cells. *Cell*. 1992;71:343–353.
3. Meir KS, Leitersdorf E. Atherosclerosis in the apolipoprotein E-deficient mouse: a decade of progress. *Arterioscler Thromb Vasc Biol*. 2004;24:1006–1014.
4. Wuttge DM, Sirsjo A, Eriksson P, Stemme S. Gene expression in atherosclerotic lesion of Apolipoprotein E deficient mice. *Mol Med*. 2001; 7:383–392.
5. Gygi SP, Rochon Y, Franza BR, Aebersold R. Correlation between protein and mRNA abundance in yeast. *Mol Cell Biol*. 1999;19: 1720–1730.
6. Mayr M, Siow R, Chung YL, Mayr U, Griffiths JR, Xu Q. Proteomic and metabolomic analysis of vascular smooth muscle cells: role of PKCdelta. *Circ Res*. 2004;94:e87–e96.
7. Mayr M, Metzler B, Chung YL, McGregor E, Mayr U, Troy H, Hu Y, Leitges M, Pachinger O, Griffiths JR, Dunn MJ, Xu Q. Ischemic preconditioning exaggerates cardiac damage in PKC-{delta} null mice. *Am J Physiol Heart Circ Physiol*. 2004;287:H946–H956.
8. Mayr M, Chung YL, Mayr U, McGregor E, Troy H, Baier G, Leitges M, Dunn MJ, Griffiths JR, Xu Q. Loss of PKC-{delta} alters cardiac metabolism. *Am J Physiol Heart Circ Physiol*. 2004;287:H937–H945.
9. Mayr M, Mayr U, Chung YL, Yin X, Griffiths JR, Xu Q. Vascular proteomics: Linking proteomic and metabolomic changes. *Proteomics*. 2004;4:3751–3761.
10. Tangirala RK, Rubin EM, Palinski W. Quantitation of atherosclerosis in murine models: correlation between lesions in the aortic origin and in the entire aorta, and differences in the extent of lesions between sexes in LDL receptor-deficient and apolipoprotein E-deficient mice. *J Lipid Res*. 1995;36:2320–2328.
11. Rabilloud T, Heller M, Gasnier F, Luche S, Rey C, Aebersold R, Benahmed M, Louisot P, Lunardi J. Proteomics analysis of cellular response to oxidative stress. Evidence for in vivo overoxidation of peroxiredoxins at their active site. *J Biol Chem*. 2002;277:19396–19401.
12. Wagner E, Luche S, Penna L, Chevallet M, Van Dorsselaer A, Leize-Wagner E, Rabilloud T. A method for detection of overoxidation of cysteines: peroxiredoxins are oxidized in vivo at the active-site cysteine during oxidative stress. *Biochem J*. 2002;366:777–785.
13. Manevich Y, Sweitzer T, Pak JH, Feinstein SI, Muzykantov V, Fisher AB. 1-Cys peroxiredoxin overexpression protects cells against phospholipid peroxidation-mediated membrane damage. *Proc Natl Acad Sci U S A*. 2002;99:11599–11604.
14. Lee SM, Koh HJ, Park DC, Song BJ, Huh TL, Park JW. Cytosolic NADP(+)-dependent isocitrate dehydrogenase status modulates oxidative damage to cells. *Free Radic Biol Med*. 2002;32:1185–1196.
15. t Hoen PA, Van der Lans CA, Van Eck M, Bijsterbosch MK, Van Berkel TJ, Twisk J. Aorta of Apolipoprotein E-deficient mice responds to atherogenic stimuli by a prelesional increase and subsequent decrease in the expression of antioxidant enzymes. *Circ Res*. 2003;93:262–269.
16. Palinski W, Ord VA, Plump AS, Breslow JL, Steinberg D, Witztum JL. Apolipoprotein E-deficient mice are a model of lipoprotein oxidation in atherogenesis. Demonstration of oxidation-specific epitopes in lesions and high titers of autoantibodies to malondialdehyde-lysine in serum. *Arterioscler Thromb*. 1994;14:605–616.
17. Shaw PX, Horkko S, Chang MK, Curtiss LK, Palinski W, Silverman GJ, Witztum JL. Natural antibodies with the T15 idiotype may act in atherosclerosis, apoptotic clearance, and protective immunity. *J Clin Invest*. 2000;105:1731–1740.
18. Palinski W, Tangirala RK, Miller E, Young SG, Witztum JL. Increased autoantibody titers against epitopes of oxidized LDL in LDL receptor-deficient mice with increased atherosclerosis. *Arterioscler Thromb Vasc Biol*. 1995;15:1569–1576.
19. Zhou X, Paulsson G, Stemme S, Hansson GK. Hypercholesterolemia is associated with a T helper (Th) 1/Th2 switch of the autoimmune response in atherosclerotic apo E-knockout mice. *J Clin Invest*. 1998;101: 1717–1725.
20. Touyz RM. Reactive oxygen species, vascular oxidative stress, and redox signaling in hypertension: what is the clinical significance? *Hypertension*. 2004;44:248–252.
21. Mayr M, Hu Y, Hainaut H, Xu Q. Mechanical stress-induced DNA damage and rac-p38MAPK signal pathways mediate p53-dependent apoptosis in vascular smooth muscle cells. *Faseb J*. 2002;16:1423–1425.
22. Khatri JJ, Johnson C, Magid R, Lessner SM, Laude KM, Dikalov SI, Harrison DG, Sung HJ, Rong Y, Galis ZS. Vascular oxidant stress enhances progression and angiogenesis of experimental atheroma. *Circulation*. 2004;109:520–525.
23. Palinski W. United they go: conjunct regulation of aortic antioxidant enzymes during atherogenesis. *Circ Res*. 2003;93:183–185.
24. Powell LA, Nally SM, McMaster D, Catherwood MA, Trimble ER. Restoration of glutathione levels in vascular smooth muscle cells exposed to high glucose conditions. *Free Radic Biol Med*. 2001;31:1149–1155.
25. Okuda M, Inoue N, Azumi H, Seno T, Sumi Y, Hirata K, Kawashima S, Hayashi Y, Itoh H, Yodoi J, Yokoyama M. Expression of glutaredoxin in human coronary arteries: its potential role in antioxidant protection against atherosclerosis. *Arterioscler Thromb Vasc Biol*. 2001;21: 1483–1487.
26. Lapenna D, de Gioia S, Ciofani G, Mezzetti A, Ucchino S, Calafiore AM, Napolitano AM, Di Ilio C, Cuccurullo F. Glutathione-related antioxidant defenses in human atherosclerotic plaques. *Circulation*. 1998;97: 1930–1934.
27. Davies KJ. Protein damage and degradation by oxygen radicals. I. general aspects. *J Biol Chem*. 1987;262:9895–9901.
28. Davies KJ, Goldberg AL. Proteins damaged by oxygen radicals are rapidly degraded in extracts of red blood cells. *J Biol Chem*. 1987;262: 8227–8234.
29. Grune T, Blasig IE, Sitte N, Roloff B, Haseloff R, Davies KJ. Peroxynitrite increases the degradation of aconitase and other cellular proteins by proteasome. *J Biol Chem*. 1998;273:10857–10862.
30. Zhang Y, Marcillat O, Giulivi C, Ernster L, Davies KJ. The oxidative inactivation of mitochondrial electron transport chain components and ATPase. *J Biol Chem*. 1990;265:16330–16336.
31. Liochev SL. The role of iron-sulfur clusters in in vivo hydroxyl radical production. *Free Radic Res*. 1996;25:369–384.
32. Opie LH. *Heart physiology: from cell to circulation.* Philadelphia: Lippincott Williams & Wilkins; 2004.
33. Lynch RM, Paul RJ. Compartmentation of glycolytic and glycogenolytic metabolism in vascular smooth muscle. *Science*. 1983;222:1344–1346.
34. Cai H, Harrison DG. Endothelial dysfunction in cardiovascular diseases: the role of oxidant stress. *Circ Res*. 2000;87:840–844.
35. Shamir R, Shehadeh N, Rosenblat M, Eshach-Adiv O, Coleman R, Kaplan M, Hamoud S, Lischinsky S, Hayek T. Oral insulin supplementation attenuates atherosclerosis progression in apolipoprotein E-deficient mice. *Arterioscler Thromb Vasc Biol*. 2003;23:104–110.
36. Bernal-Mizrachi C, Gates AC, Weng S, Imamura T, Knutsen RH, DeSantis P, Coleman T, Townsend RR, Muglia LJ, Semenkovich CF. Vascular respiratory uncoupling increases blood pressure and atherosclerosis. *Nature*. 2005;435:502–506.
37. Byk T, Ozon S, Sobel A. The Ulip family phosphoproteins–common and specific properties. *Eur J Biochem*. 1998;254:14–24.
38. Indolfi C, Avvedimento EV, Rapacciuolo A, Di Lorenzo E, Esposito G, Stabile E, Feliciello A, Mele E, Giuliano P, Condorelli G, et al. Inhibition of cellular ras prevents smooth muscle cell proliferation after vascular injury in vivo. *Nat Med*. 1995;1:541–545.
39. Leitges M, Mayr M, Braun U, Mayr U, Li C, Pfister G, Ghaffari-Tabrizi N, Baier G, Hu Y, Xu Q. Exacerbated vein graft arteriosclerosis in protein kinase Cdelta-null mice. *J Clin Invest*. 2001;108:1505–1512.

Proteomic and Metabolomic Analyses of Atherosclerotic Vessels from ApoE-deficient Mice Reveal Alterations in Inflammation, Oxidative Stress and Energy Metabolism

ONLINE SUPPLEMENT

Manuel Mayr[1], Yuen-Li Chung[2], Ursula Mayr[1], Xiaoke Yin[1], Lucy Ly[1], Helen Troy[2], Salim Fredericks [1], Yanhua Hu[1], John R. Griffiths[2], and Qingbo Xu[1]

[1] Department of Cardiac and Vascular Sciences and [2] of Basic Medical Sciences, St George´s, University of London, UK

Short title: Proteomics and Metabolomics in ApoE-/- Mice

Correspondence to:

Dr. Manuel Mayr, Department of Cardiac and Vascular Sciences, St George´s, University of London, UK, Cranmer Terrace, London SW17 0RE, UK

Tel +44 20 8725 5925

Fax +44 20 8725 2812

Email: m.mayr@sgul.ac.uk

Material and Methods

2D gel electrophoresis. Frozen aortas were pulverized under liquid nitrogen into a fine powder (n=4 per group, 3 females, 1 male). The resulting powder was dissolved in lysis buffer (9.5 M urea, 2% w/v CHAPS. 0.8% w/v Pharmalyte, pH 3-10 and 1% w/v DTT) containing a cocktail of protease inhibitors (Complete Mini, Roche) and centrifuged at 13,000 g for 10 min [1-3]. The supernatant containing soluble proteins was harvested and protein concentration was determined using a modification[4] of the method described by Bradford[5]. Solubilised samples were divided into aliquots and stored at –80°C. For two-dimensional gel electrophoresis (2-DE), extracts were loaded on nonlinear immobilized pH gradient 18-cm strips, 3-10 (GE healthcare). For analytical and preparative gels, respectively, a protein load of 100 µg and 400 µg was applied to each IPG strip using an in-gel rehydration method. Samples were diluted in rehydration solution (8 M urea, 0.5% w/v CHAPS, 0.2% w/v DTT, and 0.2 % w/v Pharmalyte pH 3-10) and rehydrated overnight in a reswelling tray. Strips were focused at 0.05 mA/IPG strip for 60 kVh at 20°C. Once IEF was completed the strips were equilibrated in 6M urea containing 30% v/v glycerol, 2% w/v SDS and 0.01% w/v Bromphenol blue, with addition of 1% w/v DTT for 15 min, followed by the same buffer without DTT, but with the addition of 4.8% w/v iodoacetamide for 15 min. SDS-PAGE was performed using 12% T (total acrylamide concentration), 2.6% C (degree of cross-linking) polyacrylamide gels without a stacking gel, using the Ettan DALT system (GE healthcare). The second dimension was terminated when the Bromphenol dye front had migrated off the lower end to the gels. After electrophoresis, gels were fixed overnight in methanol: acetic acid: water solution (4:1:5 v/v/v). 2-DE protein profiles were visualised by silver staining using the Plus one silver staining kit (GE healthcare) with slight modifications to ensure

compatibility with subsequent mass spectrometry analysis [6]. For image analysis, silver-stained gels were scanned in transmission scan mode using a calibrated scanner (GS-800, Biorad). Raw 2-DE gels were analysed using the PDQuest Software (Biorad). Normalization was performed for total spot number/volume. Differences were confirmed by an automated analysis software (Proteomeweaver, Definiens). Spots exhibiting a statistical difference in intensity in both software packages were excised for identification. For the present study, gels were processed in parallel to guarantee a maximum of comparability. Each 2-DE run was at least repeated once. All 2-DE gels were of high quality in terms of resolution as well as consistency in spot patterns.

Mass spectrometry. Gel pieces containing selected protein spots were treated overnight with modified trypsin (Promega) according to a published protocol [7] modified for use with an Investigator ProGest (Genomic Solutions, Huntington, UK) robotic digestion system. Peptide fragments were recovered by sequential extractions with 50mM ammonium hydrogen carbonate, 5% v/v formic acid, and acetonitrile. Extracts were lyophilized, resuspended in 20 µl of 0.1% v/v TFA/ 10% v/v acetonitrile, and desalted on Zip tips (Millipore) according to the manufacturer's instruction. MALDI-MS was performed using an Axima CFR spectrometer (Kratos, Manchester, UK). The instrument was operated in the positive ion reflectron mode. α-cyano-4-hydroxy-cinnaminic acid was applied as matrix. Spectra were internally calibrated using trypsin autolysis products. The resulting peptide masses were searched against databases using the MASCOT program [8]. One missed cleavage per peptide was allowed and carbamidomethylation of cysteine as well as partial oxidation of methionine were assumed. In addition to MALDI-MS, tandem mass spectrometry was performed for sequencing of tryptic digest peptides. Following

enzymatic degradation, peptides were separated by capillary liquid chromatography on a reverse-phase column (BioBasic-18, 100 x 0.18 mm, particle size 5 µm, Thermo Electron Corporation) and applied to a LCQ ion-trap mass spectrometer (LCQ Deca XP Plus, Thermo Finnigan). Spectra were collected from the ion-trap mass analyzer using full ion scan mode over the mass-to-charge (*m/z*) range 300-2000. MS-MS scans were performed on each ion using dynamic exclusion. Database search was performed using the TurboSEQUEST software (Thermo Finnigan).

Proton magnetic resonance spectroscopy (NMR). Aortas were rinsed with PBS and snap-frozen immediately in liquid nitrogen; n=5 for 10-week-old apoE +/+ mice and for 18-month-old apoE-/- mice (3 females, 2 males), n=3 for apoE-/- mice aged 10 weeks (2 females, 1 male), n=3 for 12-month-old apoE-/- mice with light and severe lesions (2 males, 1 female). Tissues were ground under liquid nitrogen using a mortar and pestle. Cell monolayers were washed twice with chilled saline after decanting the culture medium. Water-soluble metabolites were extracted in 6% perchloric acid (PCA) [9]. Adherent cells were scraped from the flasks using a cell scraper. Deproteinised extracts were transferred to ice cold centrifuge tubes and centrifuged at 3000 RPM for 10 minutes at 4°C. The supernatant was transferred to fresh cold centrifuge tubes and neutralised to pH 7 with 10M KOH. After neutralization, the cell extracts were centrifuged, the supernatant was collected, freeze-dried and reconstituted in deuterium oxide (D_2O). Immediately before the NMR analysis, the pH was readjusted to 7 with PCA or KOH. 0.5ml of the extracts were placed in 5mm NMR tubes. ^{1}H NMR spectra were obtained using a Bruker 600MHz spectrometer. The water resonance was suppressed by using gated irradiation centred on the water frequency. Sodium 3-trimethylsilyl-2,2,3,3-

tetradeuteropropionate (TSP) was added to the samples for chemical shift calibration and quantification.

Western Blotting analysis. Cellular protein extracts were harvested according to an established protocol [10, 11]. Western blotting was performed as described previously [10, 11]. Polyclonal antibodies to peroxiredoxin 1 (LF-PA0001, 1:100) were purchased from Lab Frontier. Antibodies to mouse ApoA1 and mouse albumin were obtained from Biodesign International (K23500R, 1:200) and Bethyl (A90-234A, 1:1000), respectively. Monoclonal antibodies to myosin light chain (MLM527, 1:1000) and polyclonal antibodies to catalase (ab1877. 1:100) were purchased from Abcam. The following antibodies were products from Santa Cruz: HO-1 (H-105, dilution 1:200) and SOD-1 (FL-154, 1:100).

Immunohistochemical staining. The procedure used in the present study was similar to that described previously [12]. Briefly, serial 5-µm thick frozen sections of aortic roots were overlaid with rabbit antibodies against HO-1 (Santa Cruz). Sections were incubated with horseradish-peroxidase secondary antibody conjugate and developed using the substrate solution diaminobenzidine (Dako).

Enzyme activity. Glutathione reductase activity was measured using a commercially available kit according (GR 2368, Randox Ltd., UK) on a COBAS MIRA (Roche) autoanalyser. Glutathione concentrations were measured as described previously [1, 13].

References

1. Mayr M, Siow R, Chung YL, Mayr U, Griffiths JR, Xu Q. Proteomic and metabolomic analysis of vascular smooth muscle cells: role of PKCdelta. *Circ Res.* 2004;94:e87-96.
2. Mayr M, Chung YL, Mayr U, McGregor E, Troy H, Baier G, Leitges M, Dunn MJ, Griffiths JR, Xu Q. Loss of PKC-{delta} alters cardiac metabolism. *Am J Physiol Heart Circ Physiol.* 2004;287:H937-H945.
3. Mayr M, Metzler B, Chung YL, McGregor E, Mayr U, Troy H, Hu Y, Leitges M, Pachinger O, Griffiths JR, Dunn MJ, Xu Q. Ischemic preconditioning exaggerates cardiac damage in PKC-{delta} null mice. *Am J Physiol Heart Circ Physiol.* 2004;287:H946-H956.
4. Weekes J, Wheeler CH, Yan JX, Weil J, Eschenhagen T, Scholtysik G, Dunn MJ. Bovine dilated cardiomyopathy: proteomic analysis of an animal model of human dilated cardiomyopathy. *Electrophoresis.* 1999;20:898-906.
5. Bradford MM. A rapid and sensitive method for the quantitation of microgram quantities of protein utilizing the principle of protein-dye binding. *Anal Biochem.* 1976;72:248-254.
6. Yan JX, Wait R, Berkelman T, Harry RA, Westbrook JA, Wheeler CH, Dunn MJ. A modified silver staining protocol for visualization of proteins compatible with matrix-assisted laser desorption/ionization and electrospray ionization-mass spectrometry. *Electrophoresis.* 2000;21:3666-3672.
7. Shevchenko A, Wilm M, Vorm O, Mann M. Mass spectrometric sequencing of proteins silver-stained polyacrylamide gels. *Anal Chem.* 1996;68:850-858.
8. Perkins DN, Pappin DJ, Creasy DM, Cottrell JS. Probability-based protein identification by searching sequence databases using mass spectrometry data. *Electrophoresis.* 1999;20:3551-3567.
9. Bergmeyer H. *Methods of enzymatic analysis*. Weinheim, Germany: Verlag Chemie; 1974.
10. Li C, Hu Y, Mayr M, Xu Q. Cyclic strain stress-induced mitogen-activated protein kinase (MAPK) phosphatase 1 expression in vascular smooth muscle cells is regulated by Ras/Rac-MAPK pathways. *J Biol Chem.* 1999;274:25273-25280.
11. Li C, Hu Y, Sturm G, Wick G, Xu Q. Ras/Rac-Dependent activation of p38 mitogen-activated protein kinases in smooth muscle cells stimulated by cyclic strain stress. *Arterioscler Thromb Vasc Biol.* 2000;20:E1-9.
12. Mayr U, Mayr M, Li C, Wernig F, Dietrich H, Hu Y, Xu Q. Loss of p53 accelerates neointimal lesions of vein bypass grafts in mice. *Circ Res.* 2002;90:197-204.
13. Ruiz E, Siow RC, Bartlett SR, Jenner AM, Sato H, Bannai S, Mann GE. Vitamin C inhibits diethylmaleate-induced L-cystine transport in human vascular smooth muscle cells. *Free Radic Biol Med.* 2003;34:103-110.

Online figure legend. Mass spectrometry spectra. (A) Peptide mass profiling of a silver stained spot from a 2-DE separation of aortic proteins. The protein was digested *in situ* within the gel with trypsin. The resulting tryptic peptides were analyzed using MALDI-MS in reflectron mode and identified the protein as malic enzyme supernatant, MOD-1. (B) Tandem mass spectrometry analysis of a silver stained spot from a 2-DE separation of aortic proteins. The product ion spectrum of the doubly charged tryptic peptide T-(36-46) at *m/z* 620.99 was identified as "apolipoprotein A1": (K) DFANVYVDAVK (D).

Online Figure

Mayr et al

A

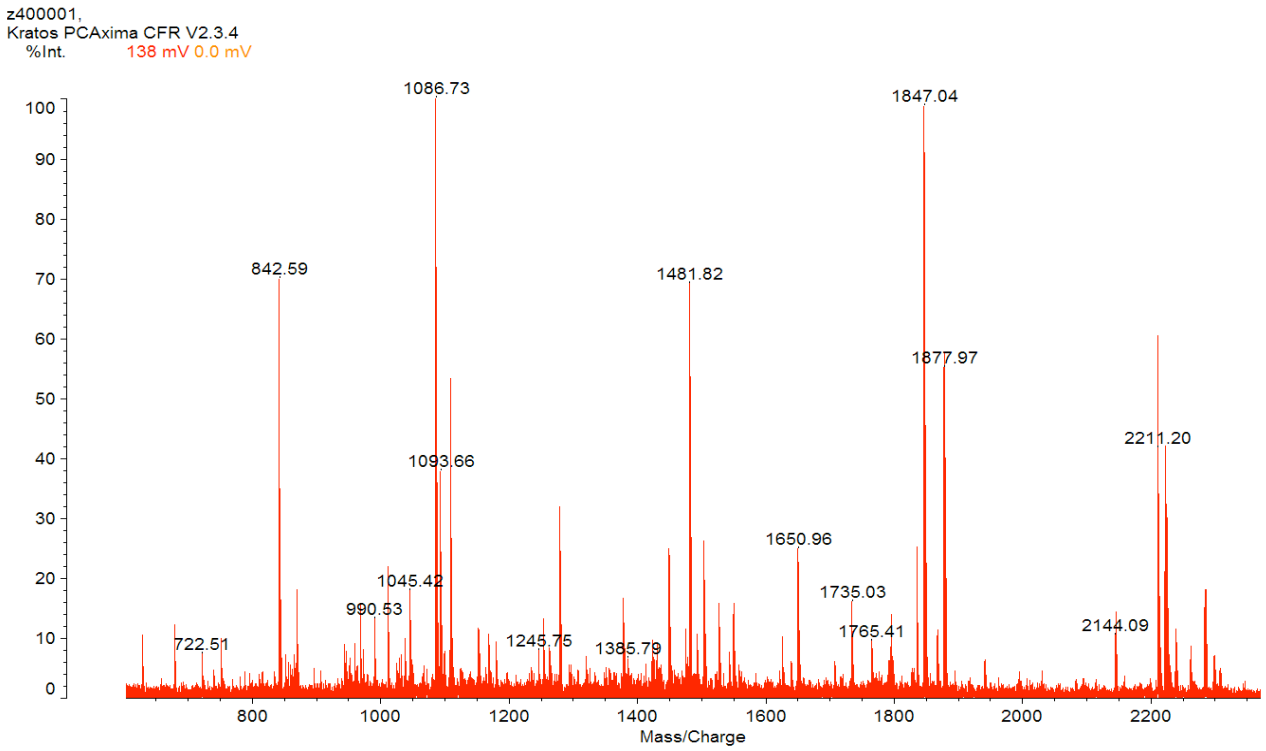

B

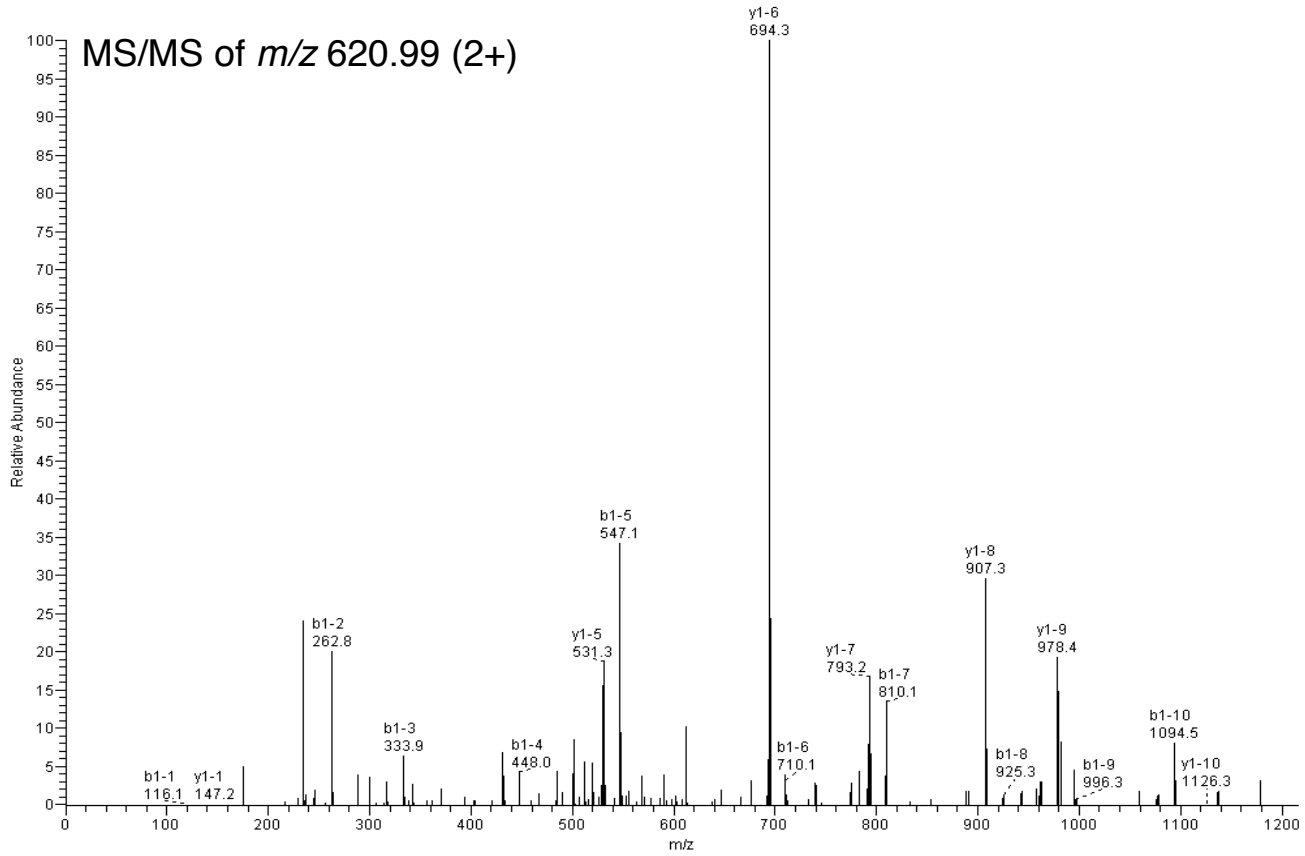

T-(36-46) D F A N V Y V D A V K

Online table I. Differentially expressed proteins in aortas derived from apoE +/+ and apoE -/- mice

N	Protein identity	NCBI entry number	Function	Calculated pI/MM Da (x10^3)	Observed pI/MM Da (x10^3)	Sequence coverage / Mascot score
	Serum components					
1	Apolipoprotein A1	6753096	Lipoprotein, HDL component	5.5 / 30.5	5.5 / 26.4	46% / 162 *
2	Immunoglobulin light chains	1127148	Immunoglobulin	7.8 / 24.1	6.1-6.8 / 25.7	29% / 66 *
3	Immunoglobulin heavy chains	26665404	Immunoglobulin	6.8 / 51.3	6.7-7.8 / 50.8	18% / 91*
4	Albumin *(fragment)*	26341396	Serum protein	5.5 / 64.9	6.5 / 30.7	22% / 70
5	Albumin *(fragment*	33859506	Serum protein	5.7 / 70.7	6.4 / 28.8	16% / 73
6	Albumin *(fragment)*	5915682	Serum protein	5.7 / 68.5	6.1 / 28.6	22% / 80
7	Albumin *(fragment)*	26341396	Serum protein	5.5 / 64.9	6.1 / 27.2	13% / 84
8	Albumin *(fragment)*	33859506	Serum protein	5.7 / 70.7	7.1 / 23.6	10% / 63
9	Albumin *(fragment)*	26986064	Serum protein	5.5 / 23.6	5.2 / 26.3	44% / 123
10	Albumin *(fragment)*	26341396	Serum protein	5.5 / 64.9	5.7 / 36.0	17% / 62
11	Albumin *(fragment)*	5915682	Serum protein	5.5 / 68.5	5.7 / 40.5	23% / 122
12	Albumin *(fragment)*	26341396	Serum protein	5.5 / 64.9	5.5 / 52.7	20% / 91
13	Albumin *(fragment)*	5915682	Serum protein	5.7 / 68.5	5.6 / 57.8	21% / 88
14	Albumin *(fragment)*	26341396	Serum protein	5.5 / 64.9	5.6 / 57.7	20% / 112
15	Albumin *(fragment)*	11277085	Serum protein	5.5 / 52.9	5.8 / 51.7	13% / 71
16	Albumin *(fragment)*	26341396	Serum protein	5.5 / 64.9	5.9 / 50.6	21% / 71
17	Albumin *(fragment)*	26341396	Serum protein	5.5 / 64.9	5.9 / 50.6	19% / 79
18	Albumin *(fragment)*	11277085	Serum protein	5.5 / 64.5	6.0 / 48.3	25% / 143
19	Albumin *(fragment)*	33859506	Serum protein	5.7 / 70.7	6.3 / 19.7	MS / MS
20	Fibrinogen, gamma polypeptide	19527078	Coagulation	5.5 / 50.0	5.6 / 53.5	10% / 62
21	Fibrinogen, gamma polypeptide	19527078	Coagulation	5.5 / 50.0	5.7 / 53.0	12% / 65
22	Fibrinogen, beta polypeptide	33859809	Coagulation	6.7 / 55.4	5.8 / 58.8	16% / 70
23	Fibrinogen, beta polypeptide	33859809	Coagulation	6.7 / 55.4	6.0 / 58.9	34% / 157
24	Fibrinogen, beta polypeptide	33859809	Coagulation	6.7 / 55.4	6.1 / 58.4	24% / 80

25	Hemopexin	23956086	Iron recovery	7.9 / 52.0	5.7 / 75.9	16% / 75
26	Transferrin	17046471	Iron transport	6.9 / 78.8	6.3 / 79.6	11% / 71
	Cell marker					
27	MAC2 antigen	126679	Galectin 3	9.0 / 27.5	8.5 / 32.1	29% / 81
28	CapG protein	13097498	Macrophage capping protein	6.5 / 39.0	6.6 / 45.0	22% / 72*
29	Transgelin, SM22 alpha	6755714	SMC differentiation marker	8.8 / 22.6	6.3 / 20.3	64% / 165
	Cytoskeleton / Myofilaments					
30	Myosin regulatory light chain 2a, MLC-2a Atrial isoform	38605071	Myofilaments	4.6 / 19.6	4.7 / 22.7	22% / 80
31	Myosin light chain 1a, MLC-1a Atrial/fetal isoform	127139	Myofilaments	4.9 / 21.2	5.1 / 24.1	24% / 84
32	Myosin light chain, alkali, Nonmuscle	33620739	Myofilaments	4.5 / 17.1	4.5 / 17.0	43% / 104
33	Myosin regulatory light chain 2, Smooth muscle isoform	38605043	Myofilaments	4.8 / 19.9	4.8 / 19.9	35% / 76*
34	Microfibrillar-associated glycoprotein 4	21313152	Microfibrils in extracellular matrix	5.2 / 29.3	5.2 / 40.3	21% / 77
35	Destrin	9790219	Actin depolymerising factor	8.1 / 18.5	6.3 / 18.9	45% / 91*
36	Vimentin	2078001	Intermediate filament	5.0 / 51.6	5.2 / 59.0	20% / 112*
37	Actin *(fragment)*	49864	Cytoskeleton	5.5 / 38.0	5.4 / 26.0	MS / MS
38	Alpha actin *(aa 40-375)*	49864	Cytoskeleton	5.4 / 38.0	5.6 / 41.6	22% / 73
39	Beta actin *(aa 27-375)*	49868	Cytoskeleton	5.8 / 39.4	5.6 / 41.6	23% / 75
40	Beta actin *(aa 27-375)*	49868	Cytoskeleton	5.8 / 39.4	5.5 / 34.3	15% / 61
41	Alpha actin *(aa 40-375)*	49864	Cytoskeleton	5.5 / 38.0	5.6 / 32.0	16% / 64
	Antioxidants					
42	Malic enzyme supernatant, MOD1	15029730	NADP-linked malate dehydrogenase	6.9 / 63.9	7.5 / 63.6	26% / 128*
43	Malic enzyme supernatant, MOD1	15029730	NADP-linked malate dehydrogenase	6.9 / 63.9	7.1 / 63.6	28% / 121*
44	1-Cys peroxiredoxin *(reduced)*	3219774	Peroxiredoxin 6, Antioxidant protein 2	5.7 / 24.9	6.1 / 27.2	37% / 90*
45	1-Cys peroxiredoxin *(oxidised)*	3219774	Peroxiredoxin 6,	5.7 / 24.9	5.9 / 27.7	25% / 73

			Antioxidant protein 2			
46	Glutathione S-transferase mu1	6754084	Conjugation of glutathione	7.7 / 26.1	8.4 / 27.6	62% / 213*
47	Peroxiredoxin 2	2499469	Thioredoxin peroxidase 1	5.2 / 21.8	5.1 / 24.6	MS / MS
	Lipid metabolism					
48	Acyl-CoA dehydrogenase, short chain specific	6680620	Beta-Oxidation of short-chain fatty acids	8.9 / 44.9	6.4 / 43.6	25% / 108*
49	Acyl-CoA dehydrogenase, short chain specific	31982522	Beta-Oxidation of short-chain fatty acids	8.7 / 45.1	7.1 / 43.5	16% / 76*
50	Acyl-CoA dehydrogenase, medium chain specific	6680618	Beta-Oxidation of medium-chain fatty acids	8.6 / 46.9	7.2 / 45.5	20% / 68
51	Acyl-CoA dehydrogenase, medium chain specific	6680618	Beta-Oxidation of medium-chain fatty acids	8.6/ 46.9	6.1 / 46.1	15% / 62
	Glucose metabolism					
52	Pyruvate dehydrogenase E1 alpha	6679261	E1 component of pyruvate dehydrogenase complex	8.5 / 43.9	7.1 / 47.0	24% / 112
53	Pyruvate dehydrogenase E1 alpha	6679261	E1 component of pyruvate dehydrogenase complex	8.5 / 43.9	6.5 / 47.2	12% / 75
54	Dihydrolipamide S-acetyltransferase E2	16580128	E2 component of pyruvate dehydrogenase complex	5.7 / 59.0	5.8 / 67.9	24% / 90
55	Dihydrolipoyldehydrogenase E3	6014973	E3 component of pyruvate dehydrogenase complex	8.0 / 54.2	6.6 / 58.7	MS / MS
56	Glyceraldehyde-3-phosphate dehydrogenase (NAD+)	3807557	Glycolytic enzyme	7.7 / 31.3	8.2 / 40.0	16% / 61*
57	Glycerol-3-phosphate dehydrogenase (NAD+)	121557	Gluconeogenesis	6.8 / 37.4	6.4 / 38.0	MS / MS
58	Triose phosphate isomerase	6678413	Glycolytic enzyme	6.9 / 27.0	7.1 / 27.0	24% / 75*
59	Enolase	119344	Glycolytic enzyme	6.7 / 47.0	6.7 / 50.1	MS / MS
60	3-Mercaptopyruvate sulfurtransferase, e	20149758	Conversion of cystein to pyruvate	6.1 / 33.2	6.1 / 33.2	22% / 107
	Energy metabolism					
61	Isocitrate dehydrogenase (NAD+), α	18250284	TCA cycle	6.6 / 39.6	5.7 / 42.9	24% / 98
62	Aconitase 2, mitochondrial	18079339	TCA cycle	8.1 / 86.1	7.7 / 74.9	8% / 72

	(fragment)					
63	Ubiquinol-cytochrome C reductase Rieske iron-sulfur polypeptide 1	13385168	Respiratory chain	8.9 / 29.6	7.5 / 26.5	14% / 82*
64	Creatine kinase muscle	6671762	Energy generation	6.6 / 43.2	6.9 / 45.5	19% / 75*
65	Malate dehydrogenase (cytoplasmic)	126889	NAD-linked malate dehydrogenase, malate-aspartate-shuttle	6.2 / 36.5	6.1 / 39.3	MS / MS
	Signalling proteins					
66	Ras suppressor protein 1	31982028	Potential inhibitor of Ras signalling	8.6 / 31.4	8.6 / 32.3	19% / 118*
67	Dihydropyrimidinase-like 2	40254595	Collapsin-response mediator 2, Ulip 2	5.9 / 62.5	5.7 / 59.8	21% / 92*
68	Dihydropyrimidinase-like 3	6681219	Unc-33-like phosphoprotein, Ulip, Collapsin-response mediator 4	6.0 / 62.3	6.2 / 69.8	MS / MS
69	Dihydropyrimidinase-like 3	6681219	Unc-33-like phosphoprotein, Ulip, Collapsin-response mediator 4	6.0 / 62.3	6.1 / 60.4	27% / 128*
70	14-3-3-protein gamma	48428722	Potential inhibitor of protein kinase C	4.3 / 28.3	4.7 / 29.7	MS / MS
	Other proteins					
71	Ubiquitin carboxyl-terminal hydrolase isoyzme L1	18203410	Ubiquitin thiolesterase, protein degradation	5.1 / 25.2	5.4 / 28.5	22% / 68*
72	Mixture:					
	1. Transketolase	730956	1. Glycolytic enzyme	7.2 / 67.6	7.9 / 67.1	MS / MS
	2. Complement C3 *(fragment)*	1352102	2. Inflammation	6.4 /186.5		
73	Mixture:					
	1. Carbonic anhydrase II	33243954	1. pH regulation	6.5 / 29.1	6.7 / 30.7	16% / 73*
	2. Phosphoglycerate mutase 1	20178035	2. Glycolytic enzyme	6.7 / 28.8		MS / MS
74	Mixture					
	1. Apolipoprotein A1	6753096	1. Lipoprotein, HDL component	5.5 / 30.5	5.6 / 26.5	MS / MS
	2. NADH ubiquinone oxidoreductase	20178012	2. Respiratory chain	7.0 / 27.3		MS / MS
75	Mixture					
	1. Osteoglycin	6679166	1. Extracellular matrix	5.5 / 34.3	5.8 / 37.4	19% / 71*
	2. Acyl-CoA dehydrogenase, short chain specific	584714	2. Lipid metabolism	8.9 / 44.9		MS/MS

76	Mixture:					
	1. Extracellular superoxide dismutase	2500824	1. Scavenger of superoxide	6.3 / 27.4	6.1 / 37.1	MS / MS
	2. Phosphatidylinositol transfer protein α	1709737	2. Catalyzes the transfer of phosphatidylinositol and phosphatidylcholine in membranes	6.0 / 31.9		MS / MS
77	Mixure:					
	1. Lamin A	1346412	1. Nuclear lamina	6.5 / 74.2	6.4 / 64.1	MS/MS
	2. T-complex protein 1 (CCT zeta)	549061	2. Actin/tubulin folding	6.6 / 58.0		MS/MS
78	Annexin A1	113945	Phospholipase A2 inhibitory protein	7.0 / 39.0	6.2 / 40.9	34% / 133
79	Prohibitin	54038837	Growth inhibition	5.6 / 29.8	5.7 / 29.1	MS / MS

pI isoelectric point, MM molecular mass, “MS/MS” denotes identification by tandem mass spectrometry

Online table II. Protein identification by tandem MS.

N	Protein identity	SWISS-PROT Entry name	SWISS-PROT acc. no.	Peptide matches	Sequence	Sequenc coverag (%)
1	Apolipoprotein A1	APOA1_MOUSE	Q00623	17	R. THVDSLR.T K. LQELQCGR.L K. DLEEVK.Q K. LQELQGR.L R. LAELK.S R. TQLAPHSEQMR.E K. SNPTLNEYHTR.A R. LGPLTR.D R. QEMNKDLEEVK.Q K. ARPALEDLR.H R. PALEDLR.H R. LSPVAEEFRDR.M K. VAPLGAELQESAR.Q K. VQPYLDEFQK.K K. VKDFANVYVDAVK.D R. DFANVYVDAVK.D R. HSLMPMLETLK.T	49.67
2	Ig kappa chain C region	KAC_MOUSE	P01837	1	R.QNGVLNSWTDQDSK.D	6.63
3	Ig gamma-1 chain C region secreted form	GC1_MOUSE	P01868	3	K.APQVYTIPPPK.E R.VNSAAFPAPIEK.T K.DVLTITLTPK.V	10.19
19	Albumin	ALBU_MOUSE	P07724	3	K.AADKDTCFSTEGPNLVTR.C R.RPCFSALTVDETYVPK.E	5.59
28	Macrophage capping protein	CAPG_MOUSE	P24452	4	R.DLALAIRDSER.Q R.YSPNTQVEILPQGR.E R.QAALQVADGFISR.M	17.74

					K.AQVEIITDGEEPAEMIQVLGPKPALK.E	
33	Myosin regulatory light chain 2-A, smooth	MLRA_RAT	P13832	2	K. GNFNY IEFTR. I R. FTDEE VDELYR. E	12.28
35	Destrin	DEST_MOUSE	Q9R0P5	1	R. YALYDASFETK. E	6.67
36	Vimentin	VIME_MOUSE	P20152	4	R. SYVTT STR. T R. ISLPLPTFSS LNLR. E R. QVQSLTCEVDALKGTNESLER. Q R. LLQDSVDFSLADAINTEFKNTR. T	13.98
37	Actin, cytoplasmic 1	ACTB_MOUSE	P60710	2	R.GYSFTTTAER.E K.SYELPDGQVITIGNER.F	6.91
42	NADP-dependent malic enzyme	MAOX_MOUSE	P06801	5	K.IWLVDSK.G R.AIFASGSPFDPVTLPDGR.T K.LFYSVLMSDVEK.F R.VRGPEYDAFLDEFMEAASSK.Y K.IKPTALIGVAAIGGAFTEQILK.D	22.20
43	NADP-dependent malic enzyme	MAOX_MOUSE	P06801	10	K.IWLVDSK.G R.AIFASGSPFDPVTLPDGR.T R.YLLLMDLQDR.N K.LFYSVLMSDVEK.F R.VRGPEYDAFLDEFMEAASSK.Y R.QQLNIHGLLPPCIISQELQVLR.I R.TLFPGQGNNSYVFPGVALGVVACGLR.H K.IKPTALIGVAAIGGAFTEQILK.D K.YCTFNDDIQGTASVAVAGLLAALR.I K.LSDQTVLFQGAGEAALGIAHLVVMAMEK.E	38.87
44	Peroxiredoxin 6 (1-Cys peroxiredoxin)	PRDX6_MOUSE	O08709	3	R.DFTPVCTTELGR.A R.NFDEILR.V R.VVDSLQLTGTKPVATPVDWK.K	28.13
46	Glutathione S-transferase Mu1	GTM1_MOUSE	P10649	4	K. RPWFA GDK.V K. ITQSN AILR.Y R. KHHLD GETEE ER.I K. VTYVD FLAYD ILDQY R. M	20.74
47	Peroxiredoxin 2	PDX2_MOUSE	Q61171	7	K.SAPDFTATAVVDGAFK.E R.KEGGLPLNIPPLLADVTK.S	37.84

					K.SLSQNYGVLK.N K.NDEGIAY.R R.GLFIIDAK.G R.QITVNDLPVGR.S R.SVDEALR.L	
48	Acyl-CoA dehydrogenase, short-chain specific, mitochondrial [Precursor]	ACDS_MOUSE	Q07417	17	R.LHTVYQSVELPETHQMLR.Q K.ELVPIAAQLDR.E K.ELVPIAAQLDREHLFPTAQVK.K R.EHLFPTAQVK.K K.QQWITPFTNGDK.I K.IGCFALSEPGNGSDAGAASTTAR.E R.EEGDSWVLNGTK.A K.GISAFLVPMPTPGLTLGK.K R.ASSTANLIFEDCR.I R.ASSTANLIFEDCRIPK.E R.IGIASQALGIAQASLDCAVK.Y R.NAFGAPLTK.L K.LQNIQFK.L K.LADMALALESAR.L R.LLTWR.A R.ITEIYEGTSEIQR.L R.LVIAGHLLR.S	47.33
49	Acyl-CoA dehydrogenase, short-chain specific, mitochondrial [Precursor]	ACDS_MOUSE	Q07417	2	R.IGIASQALGIAQASLDCAVK.Y R.ITEIYEGTSEIQR.L	8.01
55	Dihydrolipoyl dehydrogenase, mitochondrial [Precursor]	DLDH_MOUSE	O08749	9	K.ADGSTQVIDTK.N K.NQVTATKADGSTQVIDTK.N K.SEEQLKEEGIEFK.I K.NETLGGTCLNVGCIPSK.A K.TVCIEKNETLGGTCLNVGCIPSK.A K.ALTGGIAHLFK.Q R.EANLAAAFGKPINF.- R.RPFTQNLGLEELGIELDPK.G K.IPNIYAIGDVVAGPMLAH.K	30.65

56	Glyceraldehyde 3-phosphate dehydrogenase	G3P_MOUSE	P16858	4	K.VGVNG FGR.I R.GAAQN IIPAS TGAAK.A R.VPTPN VSVVD LTCR.L K.VIHDN FGIVE GLMTT VHAIT ATQK.T	18.37
57	Glycerol-3-phosphate dehydrogenase [NAD+], cytoplasmic	GPDA_MOUSE	P13707	4	R.KLTEIINTQHENVK.Y K.LPPNVVAIPDVVQAATGADILVFVVPHQFIGK.I K.ANTIGISLIK.G K.LISEVIGER.L K.VCYE GQPVGEFIR.C	22.35
58	Triosephosphate isomerase	TPIS_MOUSE	P17751	2	R.IIYGGSVTGATCK.E K.VVLAYEPVWAIGTGK.T	11.24
59	Beta enolase	ENOB_MOUSE	P21550	5	K.TLGPALLEK.K K.DATNVGDEGGFAPNILENNEALELLK.T K.LAMQEFMILPVGASSFK.E K.ACNCLLLK.V K.VNQIGSVTESIQACK.L	17.28
	Alpha enolase	ENOA_MOUSE	P17182	2	R.AAVPSGASTGIYEALELR.D V.NQIGSVTESLQACK.L	7.60
63	Ubiquinol-cytochrome c reductase iron-sulfur subunit, mitochondrial	UCRI_MOUSE	Q9CR68	1	K.EIDQEAAVEVSQLR.D	10.95
64	Creatine kinase, M chain	KCRM_MOUSE	P07310	12	K.LNYKPQEEYPDLSK.H K.VLTPDLYNK.L K.DLFD PIIQDR.H K.TDLNHENLKGGDDLDPNYVLSSR.V K.GGDDLDPNYVLSSR.V K.LSVEALNSLTGEFK.G K.SFLVWVNEEDHLR.V K.FEEILTR.L K.RGTGGVDTAAVGAVFDISNADR.L R.GTGGVDTAAVGAVFDISNADR.L R.LGSSEVEQVQLVVDGVK.L K.LMVEMEK.K	35.70
65	Malate dehydrogenase,	MDHC_MOUSE	P14152	5	K.GEFITTVQQ.R	24.71

	cytoplasmic				K.VIVVGNPANTNCLTASK.S N.VIIWGNHSSTQYPDVNHAK.V K.FVEGLPINDFSR.E K.ELTEEKETAFEFLSS.A	
66	Ras suppressor protein 1	RSU1_MOUSE	Q01730	5	K. EIGELTQLK. E K. LQILSLRDNDLISLPK. E R. ALYLSDNDFEILPPDIGKLT K. L K. NLEVLNFFNNQIEELPTQISSLQK. L K. AENNPWVTPIADQFQLGVSHVFEYI R. S	34.78
67	Dihydropyrimidinase related protein 2	DPY2_MOUSE	O08553	4	K. SAAEVIAQAR. K R. GSPLVVIVSQG K. I K. QIGENLIVPGGVK. T R. ILDLGITPGPEGHVLSRPEEVEAEAVN. R	10.66
68	Dihydropyrimidinase like protein-3	DPYL3_MOUSE	Q62188	2	R.GAPLVVICQGK.I R.AITVASQTNCPLYVTK.V	3.77
69	Dihydropyrimidinase like protein-3	DPYL3_MOUSE	Q62188	10	K.SAADLISQAR.K R.GAPLVVICQGK.I K.DNFTAIPEGTNGVEER.M R.AITVASQTNCPLYVTK.V K.AIGKDNFTAIPEGTNGVEER.M R.NLHQSGFSLSGTQVDEGVR.S R.GMYDGPVFDLTTTP.K K.NHQSVAEYNIFEGMELR.G K.AALAGG TTMIIDHVVPEPESSLTEAYEK.W R.IAVGSDSDLVIWDPDAL.K	17.97
70	14-3-3 protein gamma	1433G_MOUSE	P61982	2	R.YLAEVATGEK.R K.NVTELNEPLSNEER.N	9.56
71	Ubiquitin carboxyl-terminal hydrolase isozyme L1 (UCH-L1)	UCL1_MOUSE	Q9R0P9	4	K.NEAIQAAHDSVAQEGQCR.V K.LGVAGQWR.F K.LEFEDGSVLK.Q R.MPFPVNHGASSEDSLLQDAAK.V	25.56
72	Mixture: 1. Transketolase	TKT_MOUSE	P40142	3	R.LAVSQVPR.S R.TSRPENAIIYSNNEDFQVGQAK.V	10.75

					K.ILATPPQEDAPSVDIANIR.M	
	2. Complement C3 [Precursor]	CO3_MOUSE	P01027	3	R.VVIEDGVGDAVLTR.K R .LVAYYTLIGASGQ.R R.IFTVDNNLLPVGK.T	2.47
73	Mixture					
	1. Carbonic anhydrase II	CAH2_MOUSE	P00920	8	K.DFPIANGDR.Q R.QSPVDIDTATAHHDPALQPLLISYDK.A K.GGPLSDSYR.L K.YAAELHLVHWNTK.Y K.IGPASQGLQK.Y K.VLEALHSIK.T R.EPITVSSEQMSHFR.T	44.23
	2. Phosphoglycerate mutase 1	PGAM1_MOUSE	Q9DBJ1	2	R.TLNFN EEGDAEEAMVDNWRPAQPLK.N R.FSGWYDADLSPAGHEEAK.R R.ALPFWNEEIVPQI.K	12.60
74	Mixture:					
	1.Apolipoprotein A1 precursor	APOA1_MOUSE	Q00623	4	R.QKVAPLGAELQESAR.Q K.VAPLGAELQESAR.Q K.AQSVIDKASETLTAQ K.VKDFANVYVDAVK.D K.DFANVYVDAVK.D	29.55
	2. NADH-ubiquinone oxidoreductase 24 kDa subunit, mitochondrial	NUHM_MOUSE	Q9D6J6	1	R.DSDSILETLQR.K	20.56
75	Mixture:					
	1. Osteoglycin Mimecan precursor	MIME_MOUSE	Q62000	4	R.LEGNPIALGK.H K.HPNSFICLK.R K.RLPIGYSF R.LPIGYSF	9.06
	2. Acyl-CoA dehydrogenase, short-chain specific	ACADS_MOUSE	Q07417	1	K.IGCFALSEPGNGSDAGAASTTAR	5.58
76	Mixture:					
	1. Extracellular superoxide dismutase [Cu-Zn]	SODE_MOUSE	O09164	1	R.VQPSATLPPDQPQITGLVLFR.Q	8.37

	2. Phosphatidylinositol transfer protein α	PIPNA_MOUSE	P53810	1	R.VILPVSVDEYQVGQLYSVAEASK.N	8.49
77	Mixture:					
	1. Lamin A	LAMA_MOUSE	P48678	14	R.SLETENAGLR.L K.AAYEAELGDAR.K K.AQNTWGCGSSLR.T R.LQEKEDLQELNDR.L K.EAALSTALSEK.R K.LRDLEDSLAR.E R.NSNLVGAAHEELQQSR.I R.TALINSTGEEVAMR.K R.LADALQELR.A R.LQTLKEELDFQK.N R.IDSLSAQLSQLQK.Q R.LKDLEALLNSK.E R.IRISDSLSAQLSQLQK.Q K.AGQVVTIWASGAGATHSPPTDLVWK.A	29.61
	2. T-complex protein 1, zeta subunit	TCPZ_MOUSE	P80317	7	K.VATAQDDITGDGTTSNVLIIGELLK.Q R.IITEGFAAK.E K.ALQFLEQVK.V K.VHAELADVLTEAVVDSILAIR.K K.GIDPFSLDALAK.E K.NAIDDGCVVPGAGAVEVALAEALIK.Y K.VLAQNSGFDLQETLVK.V	18.08
79	Prohibitin	PHB_MOUSE	P67778	6	K.DLQNVNITLR.I R.IYTSIGEDYDER.V R.VLPSITTEILK.S R.FDAGELITQR.E K.AAELIANSLATAGDGLIELR.K R.KLEAAEDIAYQLSR.S	28.31

Online table III. Quantitation of Differences in Protein Profiles and Ratio to Wildtype Controls

N	Protein identity	ApoE+/+ (10 wks)	ApoE-/- (10 wks)	ApoE-/- (light)	ApoE-/- (medium)	ApoE-/- (severe)	ApoE-/- 10 wks (Ratio)	ApoE-/- Light (Ratio)	ApoE-/- Medium (Ratio)	ApoE-/- Severe (Ratio)
	Serum components									
1	Apolipoprotein A1	1326 (±147)	N.D. ***	563 * (±336)	358 ** (±128)	1099 (±173)	**0.0**	**0.4**	**0.3**	0.8
2	Immunoglobulin light chains	797 (±343)	746 (±348)	1482 (±856)	3304 * (±1218)	2866 * (±720)	0.9	1.9	**4.1**	**3.6**
3	Immunoglobulin heavy chains	475 (±198)	1415 * (±556)	1608 * (±521)	2098 * (±805)	2034 * (±557)	**3.0**	**3.4**	**4.4**	**4.3**
4	Albumin *(fragment)*	N.D.	N.D.	N.D.	417 (±162)	864 * (±210)	N.A.	N.A.	N.A.	**N.A.**
5	Albumin *(fragment)*	1787 (±73)	628 * (±256)	1999 (±339)	2879 * (±100)	3388 * (±573)	**0.4**	1.1	**1.6**	**1.9**
6	Albumin *(fragment)*	924 (±151)	555 * (±104)	1231 (±161)	1605 * (±168)	2529 *** (±244)	**0.6**	1.3	**1.7**	**2.7**
7	Albumin *(fragment)*	N.D.	N.D.	151 (±151)	355 (±240)	887* (±309)	N.A.	N.A.	N.A.	**N.A.**
8	Albumin *(fragment)*	N.D.	N.D.	N.D.	69 (±19)	206 * (±52)	N.A.	N.A.	**N.A.**	**N.A.**
9	Albumin *(fragment)*	934 (±127)	455 * (±87)	1075 (±152)	1365 (±215)	1996 * (±295)	**0.5**	1.2	1.5	**2.1**
10	Albumin *(fragment)*	373 (±76)	64 (±64)	384 (±178)	552 (±10)	587 (±179)	**0.2**	1.0	1.5	1.6
11	Albumin *(fragment)*	456 (±159)	123 (±123)	881 (±317)	1225 * (±120)	1631 *** (±175)	0.3	1.9	**2.7**	**3.6**
12	Albumin *(fragment)*	99 (±45)	33 (±33)	186 (±110)	333 (±50)	316 * (±105)	0.3	1.9	3.4	**3.2**
13	Albumin *(fragment)*	268 (±61)	259 (±107)	451 * (±51)	366 (±99)	750 * (±236)	1.0	**1.7**	1.3	**2.8**

14	Albumin *(fragment)*	291 (±73)	237 (±103)	709 ** (±40)	461 (±45)	909 *** (±104)	0.8	**2.4**	1.6	**3.1**
15	Albumin *(fragment)*	191 (±116)	61 (±35)	194 (±112)	370 (±60)	613 * (±116)	0.3	1.0	1.9	**3.2**
16	Albumin *(fragment)*	N.D.	N.D.	25 (±25)	50 (±35)	173 ** (±37)	N.A.	N.A.	N.A.	**N.A.**
17	Albumin *(fragment)*	185 (±115)	68 (±41)	145 (±67)	240 (±21)	407 * (±44)	0.4	0.8	1.3	**2.2**
18	Albumin *(fragment)*	N.D.	389 (±389)	428 (±249)	1138 (±258)	1203 ** (±349)	N.A.	N.A.	N.A.	**N.A.**
19	Albumin *(fragment)*	47 (±47)	N.D.	96 (±96)	231 (±43)	194 * (±43)	0.0	2.1	4.9	**4.2**
20	Fibrinogen, gamma polypeptide	297 (±75)	407 (±89)	1456 ** (±177)	1360 ** (±222)	1251 *** (±135)	1.4	**4.9**	**4.6**	**4.2**
21	Fibrinogen, gamma polypeptide	N.D.	N.D.	765 ** (±145)	408 *** (±79)	424 *** (±76)	N.A.	**N.A.**	**N.A.**	**N.A.**
22	Fibrinogen, beta polypeptide	N.D.	N.D.	247 * (±162)	411 *** (±161)	325 *** (±67)	N.A.	**N.A.**	**N.A.**	**N.A.**
23	Fibrinogen, beta polypeptide	1355 (±172)	971 (±271)	1779 (±303)	2896 (±663)	2478 *** (±250)	0.7	1.3	2.1	**1.8**
24	Fibrinogen, beta polypeptide	N.D.	N.D.	765 ** (±145)	408 *** (±79)	424 *** (±76)	N.A.	**N.A.**	**N.A.**	**N.A.**
25	Hemopexin	N.D.	N.D.	N.D.	N.D.	1559 * (±759)	N.A.	N.A.	N.A.	**N.A.**
26	Transferrin	896 (±206)	569 (±158)	1443 * (±52)	2063 * (±445)	1935 * (±390)	0.6	**1.6**	**2.3**	**2.2**
	Cell marker									
27	MAC2 antigen	N.D.	N.D.	322 (±195)	1073 ** (±326)	638 *** (±138)	N.A.	N.A.	**N.A.**	**N.A.**
28	CapG protein	335 (±118)	456 (±24)	852 * (±140)	827 * (±157)	848 * (±117)	1.4	**2.5**	**2.5**	**2.5**
29	Transgelin, SM22 alpha	10160	8969	10995	1884 **	7297 *	0.9	1.1	**0.2**	**0.7**

		(±1022)	(±1314)	(±2069)	(±218)	(±1138)				
	Cytoskeleton / Myofilaments									
30	Myosin regulatory light chain 2a, MLC-2a, Atrial isoform	N.D.	1056 (±551)	623 * (±155)	N.D.	N.D.	N.A.	**N.A.**	N.A.	N.A.
31	Myosin light chain 1a, MLC-1a, Atrial/fetal isoform	N.D.	1281 (±623)	813 * (±146)	N.D.	N.D.	N.A.	**N.A.**	N.A.	N.A.
32	Myosin light chain, alkali, Nonmuscle	3512 (±359)	2621 * (±199)	4097 (±452)	2852 (±95)	1584 *** (±256)	**0.7**	1.2	0.8	**0.5**
33	Myosin regulatory light chain 2, Smooth muscle isoform	6014 (±235)	5699 (±1089)	7607 * (±458)	7070 * (±121)	4049 *** (±433)	0.9	**1.3**	**1.2**	**0.7**
34	Microfibrillar-associated glycoprotein 4	3640 (±808)	5934 (±1088)	3051 (±1027)	556 ** (±151)	1587 * (±749)	1.5	0.8	**0.2**	**0.4**
35	Destrin	766 (±144)	1533 * (±288)	1116 (±125)	280 * (±57)	443 * (±103)	**2.0**	1.5	**0.4**	**0.6**
36	Vimentin	3471 (±754)	6389 * (±1105)	5372 (±2037)	3727 (±648)	2119 (±337)	**1.8**	**1.5**	1.1	0.6
37	Actin *(fragment)*	N.D.	N.D.	297 ** (± 50)	154* (± 13)	255 (± 188)	N.A.	**N.A.**	**N.A.**	N.A.
38	Alpha actin *(aa 40-375)*	1165 (±310)	1190 (±181)	3912 *** (±256)	2875 * (±537)	2708 * (±498)	1.0	**3.4**	**2.5**	**2.3**
39	Beta actin *(aa 27-375)*	566 (±165)	1042 (±185)	2660 *** (±242)	3567 *** (±420)	2698 * (±918)	1.8	**4.7**	**6.3**	**4.8**
40	Beta actin *(aa 27-375)*	193 (±118)	70 (±70)	1206 * (±135)	974 * (±196)	860 ** (±156)	0.4	**6.3**	**5.1**	**4.5**
41	Alpha actin *(aa 40-375)*	1263 (±78)	1094 (±242)	3130 *** (±245)	3287 * (±607)	2800 * (±596)	0.9	**2.5**	**2.6**	**2.2**
	Antioxidants									
42	Malic enzyme supernatant, MOD1	3333 (±764)	2474 (±486)	681 * (±155)	1511 (±158)	2184 (±420)	0.7	**0.2**	0.5	0.7
43	Malic enzyme supernatant, MOD1	906 (±220)	1186 (±510)	1667 * (±335)	890 (±194)	861 (±190)	1.3	**1.8**	1.0	1.0

44	1-Cys peroxiredoxin *(reduced)*	1469 (± 43)	437 *** (±103)	1443 (±269)	1162 (±314)	1969 (±267)	**0.3**	1.0	0.8	1.3
45	1-Cys peroxiredoxin *(oxidised)*	57 (±42)	210 * (±58)	95 (±55)	210 (±148)	347 (±201)	**3.7**	1.7	3.7	6.1
46	Glutathione S-transferase mu1	3190 (±230)	2608 (±10533)	2660 (±389)	2085 * (±146)	1946 ** (±240)	0.8	0.8	**0.7**	**0.6**
47	Peroxiredoxin 2	2921 (±875)	2379 (±729)	5029 * (±1150)	2156 (±103)	3917 (±1120)	0.8	**1.7**	0.7	1.3
	Lipid metabolism									
48	Acyl-CoA dehydrogenase, short chain specific	2824 (±425)	727 ** (±188)	2048 (±427)	2162 (±317)	2610 (±310)	**0.3**	0.7	0.8	0.9
49	Acyl-CoA dehydrogenase, short chain specific	927 (±111)	2744 *** (±180)	1142 (±192)	1024 (±174)	522 * (±213)	**3.0**	1.2	1.1	**0.6**
50	Acyl-CoA dehydrogenase, medium chain specific	960 (±139)	906 (±66)	967 (±256)	983 (±97)	1424 * (±137)	0.9	1.0	1.0	**1.5**
51	Acyl-CoA dehydrogenase, medium chain specific	437 (±150)	473 (±122)	382 (±194)	503 (±60)	1049 * (±173)	1.1	0.9	1.1	**2.4**
	Glucose metabolism									
52	Pyruvate dehydrogenase E1 alpha	1019 (±164)	511 (±298)	317 * (±191)	N.D. ***	N.D. ***	0.5	**0.3**	**N.A.**	**N.A.**
53	Pyruvate dehydrogenase E1 alpha	N.D.	725 * (±169)	639 * (±273)	526 * (±112)	814 ** (±150)	**N.A.**	**N.A.**	**N.A.**	**N.A.**
54	Dihydrolipamide S-acyltransferase E2	2717 (±528)	3127 (±393)	2478 (±266)	1794 (±374)	2019 (±514)	1.2	0.9	0.7	0.7
55	Dihydrolipoyl dehydrogenase E3	3970 (±643)	3663 (±372)	2916 (±746)	2596 (±208)	2299 * (±571)	0.9	0.7	0.7	**0.6**
56	Glyceraldehyde-3-phosphate dehydrogenase (NAD+)	4239 (±642)	1719 * (±463)	1404 ** (±145)	2782 (±122)	1848 * (±506)	**0.4**	**0.3**	0.7	**0.4**
57	Glycerol-3-phosphate dehydrogenase (NAD+)	906 (±228)	1266 (±291)	554 (±96)	232 * (±20)	1246 (±237)	1.4	0.6	**0.3**	1.4
58	Triose phosphate isomerase	2208	2245	2813	3986	4030 **	1.1	1.3	1.8	**1.8**

		(±112)	(±389)	(±275)	(±297)	(±332)				
59	Enolase	335 (±73)	688 (±232)	405 (±86)	961* (±260)	136 (±108)	2.1	1.2	**2.9**	0.4
60	3-Mercaptopyruvate sulfurtransferase, e	N.D.	420 ** (±75)	134 (±78)	86 (±60)	28 (±31)	**N.A.**	N.A.	N.A.	N.A.
	Energy metabolism									
61	Isocitrate dehydrogenase (NAD+), α	2732 (±229)	2538 (±404)	2146 (±204)	1421 ** (±71)	1828 * (±512)	0.9	0.8	**0.5**	**0.7**
62	Aconitase 2, mitochondrial *(fragment)*	239 (±24)	202 (±35)	137 * (±15)	221 (±22)	442 * (±122)	0.8	**0.6**	0.9	**1.9**
63	Ubiquinol-cytochrome C reductase *(Rieske protein)*	3925 (±395)	4171 (±478)	2434 * (±376)	8383 *** (±157)	5814 * (±834)	1.1	**0.6**	**2.1**	**1.5**
64	Creatine kinase muscle	641 (±187)	1344 (±365)	518 (±79)	2320 (±651)	52 ** (±59)	2.1	0.8	3.6	**0.1**
65	Malate dehydrogenase (cytoplasmic)	2960 (±788)	1477 * (±477)	2496 (±109)	2008 (±209)	2267 (±307)	**0.5**	0.8	0.7	0.9
	Signalling proteins									
66	Ras suppressor protein 1	2214 (±286)	1749 (±318)	1374 (±471)	1149 * (±136)	1182 * (±170)	0.8	0.6	**0.5**	**0.5**
67	Dihydropyrimidinase-like 2	669 (±91)	1012 (±190)	1101 * (±134)	182 ** (±29)	648 (±106)	1.5	**1.6**	**0.3**	1.0
68	Dihydropyrimidinase-like 3	541 (±88)	467 (±122)	422 (±68)	364 (±40)	213 (±74)	0.9	0.8	0.7	**0.4**
69	Dihydropyrimidinase-like 3	1539 (±169)	1727 (±135)	1305 (±208)	1132 (±197)	820 ** (±162)	1.1	0.8	0.7	**0.5**
70	14-3-3 protein gamma	1600 (±255)	2524 * (±335)	1872 (±362)	1043 (±100)	1496 (±143)	**1.6**	1.2	0.7	0.9
	Other proteins									
71	Ubiquitin carboxyl-terminal hydrolase isoyzme L1	550 (±102)	589 (±153)	788 (±59)	673 (±82)	1055 * (±233)	1.1	1.4	1.2	**1.9**

72	Mixture: 3. Transketolase 4. Complement C3 *(fragment)*	1023 (±211)	1398 (±503)	1725 (±322)	1357 (±112)	2676 * (±749)	1.4	1.7	1.3	**2.6**
73	Mixture: 3. Carbonic anhydrase II 4. Phosphoglycerate mutase 1	N.D.	N.D.	3333 *** (±435)	1246 (±646)	N.D.	N.A.	**N.A.**	N.A.	N.A.
74	Mixture: 1. Apolipoprotein A1 2. NADH ubiquinone oxidoreductase	1157 (±35)	1618 (±375)	2582 * (±457)	3166 * (±354)	1043 (±210)	1.4	**2.2**	**2.7**	1.2
75	Mixture 1. Osteoglycin 2. Acyl-CoA dehydrogenase, short chain specific	1159 (±161)	1090 (±228)	797 (±111)	628 * (± 66)	381 ** (± 42)	0.9	0.7	**0.5**	**0.3**
76	Mixture: 1. Extracellular superoxide dismutase 2. Phosphatidylinositol transfer protein α	155 (±68)	194 (±74)	1498 * (±423)	251 (±77)	286 (±44)	1.3	**9.7**	1.6	1.8
77	Mixure: 1. Lamin A 2. T-complex protein 1 (CCT zeta)	587 (±91)	943 (±262)	477 (±127)	636 (±73)	1474 * (±354)	1.6	0.8	1.1	**2.5**
78	Annexin A1	N.D.	N.D.	1228 *** (±135)	1555 *** (±241)	64 (±46)	N.A.	**N.A.**	**N.A.**	N.A.
79	Prohibitin	1129 (±119)	1279 (±172)	870 (±32)	522 * (±52)	979 (±163)	1.1	0.8	**0.5**	0.9

Values are absorbance units quantified by densitometry from 2D gels, bold ratios highlight significant differences compared to wildtype controls using the Student's t-test, $p < 0.05$, ** $p < 0.01$, *** $p < 0.001$, n=4 per group (3 females, 1 male). N.D., not detectable, N.A., not applicable

Online table IV. Metabolic effects of apoE deficiency in murine aortas.

	ApoE +/+ (10 wks)	ApoE -/- (10 wks)	ApoE -/- (18m)	*P* (ANOVA)
Lactate	2.739 (±0.292)	2.461 (±0.534)	2.303 (±0.270)	0.684
Alanine	0.713 (±0.108)	**0.261 (±0.039)**	0.501 (±0.094)	**0.037**
Acetate	16.530 (±2.516)	16.154 (±5.126)	13.733 (±1.430)	0.721
Glutamate	1.134 (±0.428)	0.608 (±0.165)	0.783 (±0.169)	0.532
Pyruvate	0.227 (±0.133)	0.202 (±0.081)	0.135 (±0.031)	0.771
Succinate	0.798 (±0.263)	0.239 (±0.092)	0.327 (±0.115)	0.146
Choline	0.061 (±0.010)	0.053 (±0.017)	**0.135 (±0.020)**	**0.008**
Phosphocholine	0.059 (±0.013)	0.034 (±0.008)	0.070 (±0.015)	0.283
Carnitine	0.051 (±0.016)	0.051 (±0.030)	0.040 (±0.009)	0.869
Scyllo-inositol	0.355 (±0.106)	0.187 (±0.082)	0.187 (±0.017)	0.251
Taurine	1.361 (±0.215)	0.945 (±0.086)	1.658 (±0.252)	0.168
Trimethylamine oxide	0.098 (±0.041)	0.106 (±0.055)	0.149 (±0.054)	0.729
Glycolic acid	0.354 (±0.080)	0.149 (±0.052)	0.422 (±0.119)	0.234
Total creatine	0.747 (±0.248)	0.316 (±0.043)	0.962 (±0.187)	0.164
Adenosine nucleotide pool	0.333 (±0.074)	**0.121 (±0.017)**	0.482 (±0.091)	**0.039**
Formate	10.459 (±1.269)	10.074 (±2.986)	8.158 (±1.284)	0.600

Data presented are given in μmol/g wet weight (mean±SE), n=5 for apoE +/+ aortas and for apoE-/- aortas aged 18 months (3 females, 2 males), n=3 for apoE-/- aortas aged 10 weeks (2 females, 1 male). P-values for differences between the three groups were derived from ANOVA tables (bold numbers highlight significant differences in the Bonferroni/Dunn test $p<0.017$).